The Size Evolution of Disk Galaxies in the Canada-France-Hawaii Legacy Survey

by

Anudeep Kaur Kanwar
B.Sc.H., University of Western Ontario, 2003

A Thesis submitted in Partial Fulfillment of the
Requirements for the Degree of

MASTER OF SCIENCE

in the

DEPARTMENT OF PHYSICS AND ASTRONOMY

The Size Evolution of Disk Galaxies in the Canada-France-Hawaii Legacy Survey

by

Anudeep Kaur Kanwar
B.Sc.H., University of Western Ontario, 2003

Supervisory Committee:

Dr. L. Simard, Co-Supervisor (Herzberg Institute of Astrophysics)

Dr. S. L. Ellison, Co-Supervisor (Department of Physics and Astronomy)

Dr. D. J. Schade, Joint Supervisor (Department of Physics and Astronomy)

Dr. A. Babul, Departmental Member (Department of Physics and Astronomy)

Dr. D. Andersen, External Examiner (Herzberg Institute of Astrophysics, Postdoctoral Fellow)

Supervisory Committee:

Dr. L. Simard, Co-Supervisor (Herzberg Institute of Astrophysics)

Dr. S. L. Ellison, Co-Supervisor (Department of Physics and Astronomy)

Dr. D. J. Schade, Joint Supervisor (Department of Physics and Astronomy)

Dr. A. Babul, Departmental Member (Department of Physics and Astronomy)

Dr. D. Andersen, External Examiner (Herzberg Institute of Astrophysics, Postdoctoral Fellow)

Abstract

Understanding the formation and evolution of disk galaxies remains one of the most intriguing and unsolved problems in cosmology. Despite the steady improvement in the number and quality of observations over the last decade, a clear consensus about the evolution of disks has not been reached. Using wide field data from the Canada-France-Hawaii Telescope Legacy Survey, we examine the size and surface brightness evolution of approximately 20,000 disk galaxies from $z = 0.2$ to $z = 1$. This is the largest sample size of high-redshift disk measurements to date. We perform two dimensional bulge+disk decompositions on all objects in the fields and select only those that are highly disk dominated. The size function of these disks shows that the distribution of sizes is unchanged over this redshift interval. Examination of various models of pure luminosity evolution show that there has been 0.5 $\pm$0.1 magnitudes of evolution over the redshift range $0.4 < z < 1.0$ and 1.5 $\pm$ 0.3 magnitudes of evolution over $0.2 < z < 1.0$. This is mostly consistent with passive evolution and suggests that disks were assembled prior to $z = 1$.

Table of Contents

List of Figures

List of Tables

Acknowledgements

Being in astronomy is a weird thing. Its the best subject to study, but at the same time our good friends 'Segmentation Fault' and 'NaN' seem to pay us one too many visits. Still, I can't believe how lucky I am that I get to study this stuff. But of course along with luck, comes the guidance of those around me.

First off, I would like to thank my advisors.

David, for paving the way through bureaucracy to make this possible to begin with, vouching for things when they could have been overlooked and for deeply insightful and helpful discussions.

Luc, thank you for your incredible (and admirable) diligence, both scientifically and in work ethic. Its rare that you meet someone who responds 'Yes' to the 'Are you busy?' question, but still invites you to sit down. Your broad base of knowledge makes me look forward to learning more from you in the years ahead. Thank you for everything.

To Stephen Gwyn. Re: your help on this project. Yes. T you very m for every-t. You really h-ed out. Hopefully everyone else reading this is up to par in their Kanwarese.

Thanks to Peter Stetson, for taking the time to look at my psfs, despite the frustrating IRAF interface.

To those that aren't on the island: Elliott Bryant, Joseph Postma, Beth Jack and Peng Tiao- thank you for your supportive words from afar. Your combination of humour and life advice is ridiculous (in a good way). You have each helped me immensely and I cannot quantify your worth!

Thanks to Ian McCarthy, the years you were here and the one you've been away- you truly are one of a kind and even though you're only 2 years older than me, you're the wise old man in my life.

Thanks also to Eric Peng, not only for carpooling to HIA and evenings spent

grilling burnt lamb burgers (among many other carbonized meats), but also for the unexpected science discussions which greatly helped in this project.

I can't get this far without thanking my family- my parents, brother, uncle and dog. Now that I've been living away from home for a few years, I really have learned that parents are right about a lot more things than originally thought! And this is one of those lessons that I hate to admit.

Thanks to the grad students for taking the time to 'get away' and increasing the potential energy in the sloth field.

And of course, thanks to Chris Bildfell, for proving me wrong on 'TCB', providing me with delicious (and innovative) dinners, a B.Sc.H and endless, soul-satisfying smiles.

Although taken out of context, I would like to close on the following thought from Jhumpa Lahiri. I think it can easily be applied to us astronomers. It is incredible what we're learning. This work has made realize this, and now that I am at the end of this one phase, I'm just beginning to learn.

Despite how ordinary it seems, there are times when it is beyond my imagination.

Chapter 1 | *Introduction*

1.1 Prologue & Early Views

The evolution of galaxies in the universe proceeds in the most natural manner. Early galaxies are thought to be small and irregularly shaped. Over time, interactions with other galaxies allows them to grow into large, majestic spirals and ellipticals. In these often violent processes, many of the initial features are lost and the original morphology is rarely preserved. This makes it difficult to follow the evolution of a single galaxy on its own. In order to create a picture for the evolution of galaxies, one needs to observe many galaxies at different stages in their histories. Thankfully the universe naturally lends itself to this type of study, as distant observations reveal the state of objects as they were billions of years ago.

The morphology of a galaxy is the most accessible way of identifying its history of interaction. Although a given morphology may be acquired in several different ways, some simple cases can be considered to piece together a possible history. Elements of a galaxy's past can be inferred from the presence of certain tell-tale structures. One prominent feature suggesting a recent interaction is the presence of long tidal tails stretching out from the central structure of a galaxy. More stable forms can also be traced in a similar way, as a spheroidal galaxy is thought to arise from the union of two similarly massive galaxies. It is through these types of collisions that a myriad of galaxy morphologies are possible.

Over the course of its history, a galaxy will endure many stages through these interactions. Thus, the morphology of a galaxy is essentially only a transient prop-

erty. Although there is no set path for galaxy evolution, the history of a disk galaxy is thought to be significantly simpler than others. Formation theories pin them as the primary stage of galaxy evolution. In this way, they provide an excellent constraint for understanding galaxy formation and evolution in the universe, as their mere presence reveals that they may be mostly untouched. Large disks can form by accreting nearby gas onto their small primordial form, thereby increasing the galaxy's radial size. Disks that have survived to the present day are large, as they have had the longest time to acquire material in this relatively quiet manner. It is also possible for a disk to form after a major merger, growing around a central bulge component. The relative sizes of the components depends on the gas content of the progenitors (Robertson et al, 2006, Springel & Hernquist, 2005). Disk galaxies make up approximately 60-80% of the nearby population of galaxies (Buta et al, 1994) therefore the understanding of their formation has the potential to significantly advance the understanding of galaxy formation in general.

The root of the theory of galaxy formation rests within the Lambda Cold Dark Matter (ΛCDM) cosmology, wherein most of the mass of the universe is tied up in an unknown form, detectable only by gravitational means. Although the ΛCDM cosmology has witnessed many triumphs over recent years, forming disk galaxies within the framework has consistently been met with discord. Simulated disks are found to be smaller than their observed counterparts predict for a given rotation speed (e.g. Abadi et al, 2003) and early formation epochs for the galaxy allow more time for a collision which may disrupt the fragile disk structure. The violent nature of the ΛCDM hierarchical framework is then faced with an interesting challenge to the formation of disks- the most abundant galaxy type in the universe.

Initially it was believed that our own galaxy was formed through the rapid, monolithic collapse of a large, rotating gas cloud. This was first proposed in the work by Eggen, Lynden-Bell & Sandage, 1962 (ELS). They observed the motions of old stars and the distribution of metals in the Galaxy. This led them to propose

a formation model in which a large gas cloud experienced a primary contraction approximately 10^{10} years ago. As the cloud collapsed, stars began to condense out of the material. This began with the formation of stars in globular clusters in the Galactic halo. The collapse of the cloud was halted in the radial direction as it became balanced by rotational support, but continued perpendicular to the plane resulting in the formation of a thin disk.

Although this model does provide a general solution, there are some important details that it fails to satisfy. Some of these points were raised in a later study by Searle & Zinn, 1978. In their work, they abandoned the monolithic collapse model and postulated that the Galaxy was formed by the mergers of small fragments that could be used to create the halo. This was motivated by their own observations of the metallicity distribution, which they found to be inconsistent with the predictions of the monolithic collapse model. They found that the Galaxy did not exhibit a metallicity dropoff beyond eight kiloparsecs which did not agree with the ELS prediction of a steady dropoff from the central region outward. In addition, the ELS model fails to explain the presence of stars on retrograde orbits. The idea behind the 'fragment' model is that it will allow for objects with different properties to enter the system. For example, it is thought that part of the Milky Way galactic halo may have been formed by the accretion of small metal-poor satellites. The model of Searle & Zinn was eventually expanded from 'halo fragments' to whole other galaxies to form the basis of the hierarchical model for galaxy formation.

1.2 Theory

1.2.1 Galaxy Formation

The details of galaxy formation are dependent on the cosmological parameters that govern the universe. In the currently favoured theory for galaxy formation, structure is built hierarchically. The hierarchical model arises naturally from the Cold

Dark Matter cosmology in which objects, namely dark matter haloes, are created on smaller scales. Within these haloes, smaller 'building block' type galaxies are formed. Larger objects are then formed through the conglomeration of many smaller ones. Hot or warm dark matter theories postulate that structures proceed in the opposite manner; the initial masses formed are very large 'pancake-like' structures and smaller objects such as galaxies and galaxy clusters fall out as fragments (Blumenthal et al, 1984). However, this fragmentation is thought to occur very late in the universe's history ($z \approx 2$), and this is inconsistent with observations that show that many galaxies are already in existence at this epoch (eg. Steidel et al, 2003, Labbé et al, 2003). Therefore, galaxy formation is thought to proceed in the 'bottom-up' manner, from smaller to larger, as opposed to the 'top-down' fragmentation model.

Fall & Efstathiou, 1980 proposed a model for galaxy formation in which gas cools and condenses within a cold dark matter halo. The halo itself acquires angular momentum through tidal torques with other halos and the gas contained within the halo is assumed to have some fraction of the angular momentum. This model begins with an idea simliar to that of ELS; that the collapse of a large gas cloud is the principal formation mechanism. Fall & Efstathiou took this idea somewhat further. They added that this collapse occurs within a massive halo and that these halos are formed through hierarchical clustering with others. As the gas within the halo collapses into a disk, the disk is able to support itself through its rapid rotation. In order for the galaxy to collapse, much of the initial energy of the gas must be dissipated. This is because a disk galaxy is a cool, condensed structure. There are four important cooling mechanisms in galaxy formation: (1) compton cooling, (2) bremsstrahlung, (3) recombination and (4) collision induced de-excitation (Silk & Bouwens, 2006). The relative importance of these mechanisms depends on the temperature and mass of the parent dark matter halo, as well as the redshift. As energy from the halo is dissipated, stars are able to form out of cooled gas in the

plane of the disk. This forms the basic, primordial disk.

Over time, these small disks will merge with others. After a number of minor mergers, the disk will grow substantially larger, and some of the mass will begin to collect in the centre of the galaxy to form a bulge. In the ΛCDM paradigm, the formation of disks is expected to follow this 'inside-out' formation. It is also possible for the system to grow by accretion of nearby gas, although this may be slower method of growing than discrete merging events (depending on accretion rates, which vary with redshift). Upon merging with a similarly massive galaxy, an elliptical may be formed if the progenitors are sufficiently gas-poor. Recent studies show that the resultant morphology is sensitive to the quantity of gas present in the constituents (Robertson et al, 2006, Springel & Hernquist, 2005). 'Wet' or gas-rich mergers may have several possible outcomes, some of which will consist of a significant disk component.

1.2.2 Predictions on the Size & Surface Brightness Evolution of Disk Galaxies

Size is a fundmamental parameter in the understanding of galaxy evolution. By tracing the sizes of galaxies through redshift, one can infer how structures grow through cosmological time. In addition, disk galaxies provide particularly useful attributes: (1) they are the most basic type of galaxy in the universe, (2) their size measurement is relatively straightforward, and (3) they exist across all redshifts. Thus, they can be used as an indicator of growth of structures in the universe.

Within the context of the ΛCDM cosmology, there have been a number of models over the last decade attempting to understand the size and surface brightness evolution of disk galaxies. Disk galaxies are a powerful test of the hierarchical model. Our current theory of galaxy formation presumes that all galaxies begin as small disks. They are the simplest, regular form of galaxy that exist in the universe across all cosmological times. Both these factors of constancy in time and shape allow for

isolation in detecting any changes to this form. In addition, measuring the size of a galaxy is the most robust and straightforward parameter to measure.

One of the most recent analytic models for disk formation is by Mo, Mao & White, 1998. They use the standard Press-Schechter formalism to calculate the number of initial dark matter haloes (Press & Schechter, 1974). This widely used formalism is used to predict the number of virialized haloes assuming an initial distribution of density perturbations. The formula gives the number of haloes in a given mass range, M to $M+dM$, as a function of redshift. Mo, Mao & White, 1998 also make a number of other assumptions that link the disk properties to those of its parent dark matter halo, similar to Fall & Efstathiou, 1980. The mass of the disk is some fixed fraction of the halo (m_d), as is the angular momentum (j_d). The disk itself is a thin structure that is supported by its rotation and is a dynamically stable system under the right conditions. Since the early universe was more dense, galaxies at high redshift are predicted to be smaller and denser than those of the present time. Specifically, Mo, Mao & White, 1998 predict that disk sizes should scale as:

$$R_d(z) = \frac{1}{\sqrt{2}} \left(\frac{j_d}{m_d} \right) \lambda r_{200} \tag{1.1}$$

$$= 8.8 h^{-1} kpc \left(\frac{\lambda}{0.05} \right) \left(\frac{V_c}{250 km/s} \right) \left(\frac{H_0}{H(z)} \right) \left(\frac{j_d}{m_d} \right)$$

where λ is the spin parameter of the parent dark matter halo, V_c is the circular velocity. Expressed as fractions of the halo properties, j_d is the angular momentum of the disk and m_d is the mass of the disk. H_0 is the current value of the Hubble constant, and $H(z)$ is the Hubble constant at redshift z defined as:

$$H(z) = H_0[\Omega_\Lambda + (1 - \Omega_\Lambda - \Omega_M)(1+z)^2 + \Omega_M(1+z)^3]^{1/2} \tag{1.2}$$

The above equations illustrate that disk size through redshift is directly proportional to the ratio of the current Hubble constant to the Hubble constant at time z. In

turn, this fraction depends on the values of Ω_M and Ω_Λ. Out to $z = 1$, $H(z)$ is found to be approximately 1.8 times its current value (using $\Omega_M = 0.27$ and $\Omega_\Lambda = 0.7$), thus disk sizes should be 1/1.8, or 56% of their current size.

In equation 1.1, r_{200} is defined as the radius within which the mass density of the halo is 200 times the critical density needed for a closed universe at the given redshift. Since the critical density ($\rho_{crit} = 3H_0^2/8\pi G$) depends on H_0 and r_{200} depends on $H(z)$:

$$r_{200} = \frac{V_c}{10H(z)} \tag{1.3}$$

a similar argument to that presented above yields that disks should be more dense at higher redshifts. These models claim that large disk galaxies are stable within the ΛCDM cosmology provided that they have assembled the bulk of their mass in the last 8 billion years (since $z \approx 1$).

Another work by van den Bosch, 1998 also found that stable disk dominated galaxies would only be able to form in a dark-matter dominated universe if they have late formation redshifts ($z \leq 1$). If they form earlier, they are expected to contain a significant bulge component. Bouwens, Cayòns & Silk, 2002 use an inside out formation model for a number of different morphologies and find that disks have undergone an evolution in both size and surface brightness since $z \approx 1$. Their infall model predicts a brightening of approximately 1.2 magnitudes over this redshift range and a net decrease in the number of large galaxies by about 29% in an $\Omega = 1$ cosmology. In a later work, Bouwens & Silk, 2002 presented another model in which they found that disk galaxies have undergone a B-band surface brightness evolution of about 1.5 magnitudes over the $0 < z < 1$ redshift range.

1.2.3 Simulations of Disk galaxies

In addition to purely analytic modelling, many numerical (N-body) simulations are used to understand the evolution of disks. A series of high resolution N-body sim-

ulations by Steinmetz & Navarro, 2002 incorporated star formation and feedback to examine histories of various galaxy morphologies. In their simulations, pure disk galaxies were formed through the cool gas collecting at the centre of their dark matter haloes, and spheroidal galaxies were built up through the mergers of large disk galaxies. Thus, through a combination of mergers and accretion one can produce the essential components of galaxies that are observed in the universe today. One of the key points of this study is that any galaxy in the local universe will have gone through a number of transient states to arrive at its observed morphology.

Later, Abadi et al, 2003 performed a high resolution simulation specifically examing the formation of disk galaxies in a ΛCDM framework. They were able to successfully reproduce many of the observed characteristics of disk galaxies such as the surface brightness of both the bulge and disk components, the colour gradient based on the ages of constituent stars and the photometry closely matched that of a barred Sa galaxy. The simulation was unable to reproduce the correct magnitude-velocity, or Tully-Fisher relationship. For a given rotation speed, a disk will be approximately 1 magnitude brighter than the prediction of the simulation. Steinmetz & Navarro, 1999 also found the same problem. This problem occurs in many simulations and is attributed to the angular momentum distribution in the system. It is found that baryonic components of the galaxy transfer too much of their angular momentum early in their formation, resulting in a dense, slowly rotating spheroid. Steinmetz & Navarro, 1999 find that some sort of heating mechanism must be invoked prior to mergers with other systems to prevent the loss of angular momentum to the luminous component before it is fully formed.

1.3 Observations

1.3.1 Current Status

Over the last ten or so years, there has been an abundance of space and ground-based observations of disk galaxies. With the advent of larger and deeper surveys, the statistics and quality of the observations have improved vastly. Vogt et al, 1996 found that large, massive disk galaxies were in place by $z \approx 1$ using a sample of only 16 galaxies. Later Roche et al, 1998, used a more sizeable sample of 347 objects and found that disks have undergone a surface brightness evolution of approximately 0.95 magnitudes over $0.2 < z < 0.9$. In addition, they found that disks have also undergone some size evolution over this time period. Using 341 objects selected from the Canada-France-Hawaii Redshift survey, Lilly et al, 1998 found that the size function of larger disks (h $> 3.2h^{-1}$ kiloparsecs) is approximately constant to $z \approx 1$ and that disks were approximately 0.8 magnitudes brighter at $z = 0.7$. Using data from the Deep Extragalactic Evolutionary Probe (DEEP), Simard et al, 1999 performed a careful analysis of selection effects and found that there has been no evolution in disk surface brightness using their sample of 190 field galaxies.

In somewhat more recent times, sample sizes have tipped past one thousand and statistical precision should help to clarify the disagreements noted above. Ravindranath et al, 2004 used 1508 galaxies from the Great Observatories Origins Deep Survey (GOODS) and also found that there has been no evolution in the surface brightness of disks over the redshift range $0.2 < z < 1.25$. However, a recent work by Barden et al, 2005 used 5664 disks from the Galaxy Evolution from Morphologies and SEDs (GEMS) survey and found that there has been a brightening of approximately 1 magnitude out to $z \leq 1.1$.

1.3.2 This Work

Although sample sizes have improved, there is still much debate as to the evolution, or lack of evolution, of disks out to $z = 1$. In this study, data from the Deep Synoptic Component of the Canada-France-Hawaii Telescope Legacy Survey (CFHTLS) is used to examine the size and surface brightness evolution of disk dominated galaxies to $z \approx 1$. An initial sample of approximately 400,000 galaxies is obtained from two Legacy Deep fields, each of which cover approximately one square degree. Although previous studies have sought to answer this question in the past, such work has never been done with the vast sample size inherent to the CFHTLS. Since it is impossible to watch any single galaxy evolve in a lifetime, one must piece together snapshots of different galaxies in order to create a plausible evolutionary picture. The study of galaxy evolution is then much better understood with large enough sample sizes to examine this progression smoothly. The CFHTLS is one of the best data sets available to perform this task to $z \approx 1$.

This thesis is organized into five chapters. Chapter 2 provides a description of the data as well as the basic reduction techniques and methodology. In Chapter 3, the scientific analysis is described, and results are presented. In Chapter 4, the results from this work are discussed with respect to other observations as well as theoretical modelling. In Chapter 5, a summary of the results of this thesis is presented as well as prospects for future work. Throughout this thesis, concordance cosmology ($h = 0.71, \Omega_\Lambda = 0.73, \Omega_M = 0.27.$) is used.

Chapter 2 | *Data and Methods*

2.1 Data Reduction & Computations

2.1.1 Description of the sample

The data used for this thesis was obtained as part of the Deep component of the Canada-France-Hawaii Telescope Legacy Survey. The CFHTLS is a large five year project that began in 2003*. The overall goal of the Deep survey is to obtain a better understanding of the early universe through detection of thousands of supernovae and the study of the galaxy population. Covering four square degrees, the survey hopes to use large statistical samples to build stronger constraints on galaxy evolution and the star formation history of the universe.

The large survey area is possible due to the wide field camera MegaCam. The charge coupled device (CCD) camera MegaCam was mounted as part of a new prime focus system for the CFHT for the purpose of this survey. MegaCam consists of a mosaic of a 9 by 4 array of CCDs . There are also 4 chips on the edges of the CCD of the middle rows that are used for guiding the telescope. With an average scale of 0.187"/pixel, each CCD in the mosaic has 2048 x 4612 pixels. The detector has a field of view of approximately 0.96 deg x 0.94 deg. † Table 2.1 outlines the different exposure times in each filter. The morphological analysis was performed using the i' band images, and the other bandpasses were used in the computation of photometric redshifts.

*http://www.cfht.hawaii.edu/Science/CFHLS/

†http://www-dapnia.cea.fr/Phys/Sap/Activites/Projets/Megacam/page.shtml

2.1.2 Method

Basic pre-processing is performed using the ELIXIR pipeline at CFHT (Magnier & Cuillandre). At this level, the bias and overscan are subtracted, bad pixels are masked, fringe and flatfield corrections are performed as well as the computation of the first order astrometric solution for each CCD. The astrometric solution is then computed to 2nd order using the `astrogwyn` procedure[‡]. The images are then stacked using SWarp, a procedure designed to stack wide-field optical images.

Sources are extracted using the SExtractor routine (Bertin & Arnouts, 1996), and a catalogue of objects is generated. This basic catalogue provides positions, various flags and a stellarity index for every object detected in the image. Basic photometry in all 5 bands was done using Kron-style apertures in SExtractor's double image mode. Upon calculation of photometric redshifts (§ 2.1.3), absolute magnitudes were calculated for each object as in previous studies (Nüijten et al, 2005). The procedures mentioned above were performed by a collaborator of this study, S. D. J. Gwyn.

The point spread function of the images was built using the DAOPHOT (Stetson, 1987) package within the Image Reduction and Analysis Facility (IRAF). A variable moffat type point-spread function was constructed for each chip. Typical

[‡]Procedures are outlined at `http://www.astro.uvic.ca/grads/gwyn/cfhtls/index.html` and pages therein.

Table 2.1: Number of exposures and times in each bandpass for D1 & D3

Band	λ range Å	*Number* [D1]	t (secs) [D1]	*Number* [D3]	t [D3]
u*	3000 - 5540	16	10560	9	5940
g'	3720 - 6100	41	8280	35	6300
r'	5100 - 7220	64	23040	64	14600
i'	6580 - 9120	96	49920	150	46740
z'	7780 - 10240	30	10800	20	3600

full-width-half maximum was approximately 0.95", although it was adjusted from chip-to-chip. Chips further from the center of the mosaic generally had larger values for the full-width-half maximum than those near the center, but they never deviated by more than 10% from this value. On a given chip, the variability of the point spread function was also modelled by DAOPHOT. A 'true' point spread function was modelled for the entire chip, but several lookup tables were computed to measure deviations from this model. For this data, the point spread function was allowed to vary quadratrically over the chip. Terms were proportional to $1, x, y, x^2, xy$ and y^2 where x and y are positions on the chip. The choice of the moffat function to fit the stellar profile is fairly common. It is known to be numerically well behaved in fitting narrow point spread functions and also the wings fit stellar profiles better than a gaussian profile (Trujillo et al, 2001).

The radius used to fit the point spread function was 5.6"-6". Larger values were found to contaminate the point spread function with neighbours, and smaller values did not provide a good model of the innermost pixels. Generally, 75 point source objects were used to generate the model point spread function for each chip. These objects were selected provided they passed for a stellar type object based on their SExtractor stellarity index and that they appeared to be fairly well isolated, in focus with regular, circular isophotes. The process of building the point spread function was iterated for every image until a satisfactory result was obtained as evaluated by visual inspection. Objects are convolved with the model point spread function and subtracted from the original image. A good model of the point spread function will subtract fairly cleanly from the image with no systematics present. Systematic errors for the point spread function include a very bright or dark spot in the center of the object or dark spots within the point spread function's fitting radius. Once these systematics are eliminated, the point spread function was tested in the fitting routine, and minor adjustments were made if necessary.

After determining the point spread function, the following procedures were per-

formed to arrive at the size function. Each of these steps are described in more detail in the following subsections. The point spread function is used in the fitting routine to determine the morphology of the galaxy as described in section 2.2. Disk dominated galaxies are then selected from the whole sample as outlined in section 2.3. A unique identification based on SExtractor coordinates is used to look up the galaxy in the pre-existing catalogue that contains photometric redshifts ($\oint$ 2.1.3) and apparent and absolute magnitudes. From the redshift and the measurements from the fitting routine, the scale length and accessible volumes are computed for each galaxy ($\oint$2.1.4). Along with luminosity measurements, these values are then used to compute the size function ($\oint$2.5) for further analysis ($\oint$2.6).

2.1.3 Photometric redshifts

Photometric redshifts were computed with the `gwynz` procedure developed by S. D. J. Gwyn.[§] using broadband photometry for each galaxy in the field. This is done by creating a low resolution spectral energy distribution using all of the rest frame *u*,g',r',i',z'* colours, multiplying by the MegaCam filter response curve and comparing the spectra to a known galaxy template spectra. The best matching template is the one that yielded the lowest value of χ^2. This particular method of computing photometric redshifts is known as the template fitting method. This method does require a fairly good understanding of various galaxy template spectra. Thankfully, this has been modelled quite well. The templates used in this thesis are those of Coleman, Wu & Weedman, 1980. Using a suitable galaxy template, the galaxy spectral energy distibution (SED) is shifted by some amount in λ until the distribution matches the template (Figure 2.1). The best fit is an overall agreement between the galaxy SED and the template. From the measured $\Delta\lambda$, one can then

[§]Ibid

compute the redshift of the galaxy from the standard redshift relation:

$$z = \frac{\lambda - \lambda_0}{\lambda_0} \tag{2.1}$$

where λ_0 is the rest wavelength of the feature in the galaxy's spectrum, and λ is the measured wavelength. For the case of template fitting, there is not one particular 'feature' that is used for λ_0, as it can be determined from several features of the spectrum. The overall agreement between the galaxy SED and the template (determined from the lowest χ^2 value) will provide the best value of $\Delta\lambda$ (Gwyn, 1995). This gives both the redshift of the galaxy and the galaxy spectral type. Although this method does not rigorously capture the galaxy spectrum as well as a spectroscopic observation, it is generally found that the relative error in the photometric redshift measurements is about $\delta z/(1+z) = 0.11$ (Nüijten). Thus, it is very appropriate to use photometric redshifts for large samples. It is important to note that the photometric redshift routine used in this study was constrained to return redshift values between 0 and 1.5. Due to this constraint, higher redshift objects may be assigned erroneous redshifts as described in section 2.4.

2.1.4 Maximum/Accessible Volumes

The $1/V_{max}$ method is used to compute weighted number densities as outlined by Schmidt, 1968. The accessible volume of a galaxy is defined as the comoving cosmological volume that a galaxy may occupy and continue to remain within the selection criteria of the survey. The sample is subdivided into a number of redshift shells, $0.2 \leq z < 0.4$, $0.4 \leq z < 0.6$, $0.6 \leq z < 0.8$ and $0.8 \leq z < 1.0$. The boundaries of the corresponding cosmological volumes are set by the redshift limits z_{min} and z_{max} of the galaxy. These maximum redshifts are determined by the magnitude limit of the survey which was set to be i'=24.5. This limit was set by the reliability of the scale length measurements, both from simulations ($\oint$ 2.2.1) and the fractional error (h_{err}/h_d) of the measurement from the routine. One can

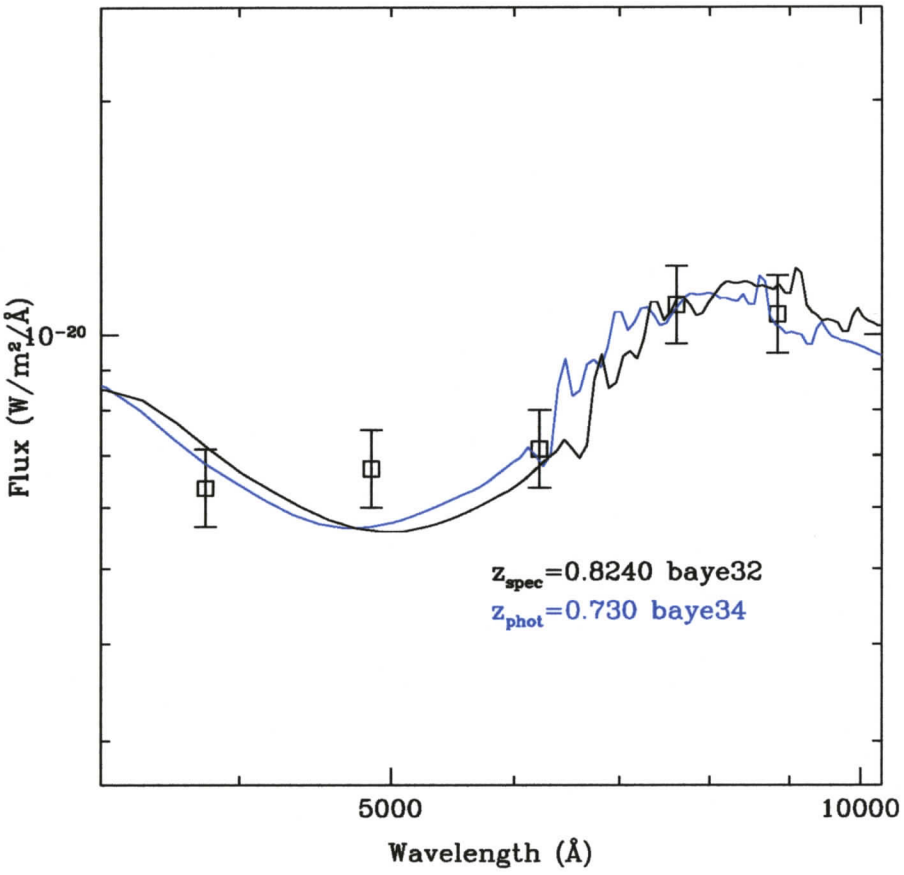

Figure 2.1:

An example of template fitting for determining a photometric redshift: The data points show the galaxy spectral energy distribution as determined by photometry. The solid blue line indicates the nearest galaxy template fit, which has been shifted in wavelength in order to match up with the galaxy spectral energy distribution. Also indicated is the spectroscopic redshift of the galaxy. Following each redshift value is the name of the galaxy template.

then compute the maximum redshift that the galaxy could have and remain in the sample. If the maximum redshift of a galaxy exceeds the upper bound of its shell, the upper bound is taken to be z_{max}. The lower bound of visibility is the lower bound of the redshift bin of the galaxy. Using these values one can integrate the comoving volume element between these redshift limits for each galaxy:

$$dV_C = D_H \frac{D_C^2}{\sqrt{\Omega_M(1+z)^3 + \Omega_\Lambda}} d\Omega dz \tag{2.2}$$

where D_H is the Hubble distance, defined as $\frac{c}{H_0}$; where H_0 is the Hubble constant $d\Omega$ is the solid angle element on the sky, for each field in the survey $d_\Omega = 0.9/41253$. D_C is the comoving distance defined as

$$D_c = D_H \int_{z_{low}}^{z_{max}} \frac{dz}{\sqrt{\Omega_M(1+z)^3 + \Omega_\Lambda}} \tag{2.3}$$

where Ω_M is the parameter for matter density in the universe, and Ω_Λ is the cosmological constant. (The above are adopted from Hogg, 2000 in the case where Ω_K is 0.) From this, it can be seen that faint galaxies (while numerous) will naturally occupy a small accessible volume as they are likely not visible throughout an entire redshift shell. Bright galaxies are easier to detect and are visible through larger volumes of space.

2.2 The fitting routine

Two-dimensional bulge + disk decomposition conveys the idea that most galaxies can be thought of as containing both a bulge and disk component. Using digitized images, one can analyze the distribution of light in a galaxy and upon understanding the point spread function of the image, fit the profile to idealized, convolved models. This technique has been used extensively in the past (Simien & de Vaucouleurs, 1986, Kent, 1984) and continues into the present day (Peng et al, 2000, Simard et

al, 2002). This type of analysis allows for insight into the different morphologies present across cosmological time and the potential to piece together the evolutionary history of galaxies through their morphology.

Using a two component analysis is extremely useful in determining the fraction of light in each of the bulge and the disk. However, in cases where one component is strongly dominating the other, it is useful to just use a pure bulge or disk model. Two-dimensional bulge + disk decomposition is performed to analyze the surface brightness profile of over 400,000 galaxies. Of these, approximately 100,000 can be identified as disk dominated galaxies (with a magnitude cut of i' <24.5) as described in the following section. We used the surface brightness fitting routine GALFIT (Schade et al, 1995) which uses a modified Levenberg-Marquardt χ^2 minimization routine to fit a number of different models to galaxy images.

The Bulge model

The surface brightness profile of the bulge component of a galaxy can be described by a deVaucoleurs profile (Binney & Tremaine, 1987). The bulge component of a galaxy usually contains older, redder stars with little or no new stars being formed. The profile is defined as:

$$\Sigma(r) = \Sigma_e exp[-7.67((r/R_e)^{1/4} - 1)] \tag{2.4}$$

where Σ_e is the effective surface brightness of the bulge, $\Sigma(r)$ is the surface brightness at some r, and R_e is bulge effective radius defined as the radius within which half the light of the spheroid is contained.

The Disk model

The disk component of a galaxy typically contains younger, bluer stars and a gaseous component which allows for replenishment of the stellar supply. The surface brightness of the disk component of a galaxy can be described by an exponential profile

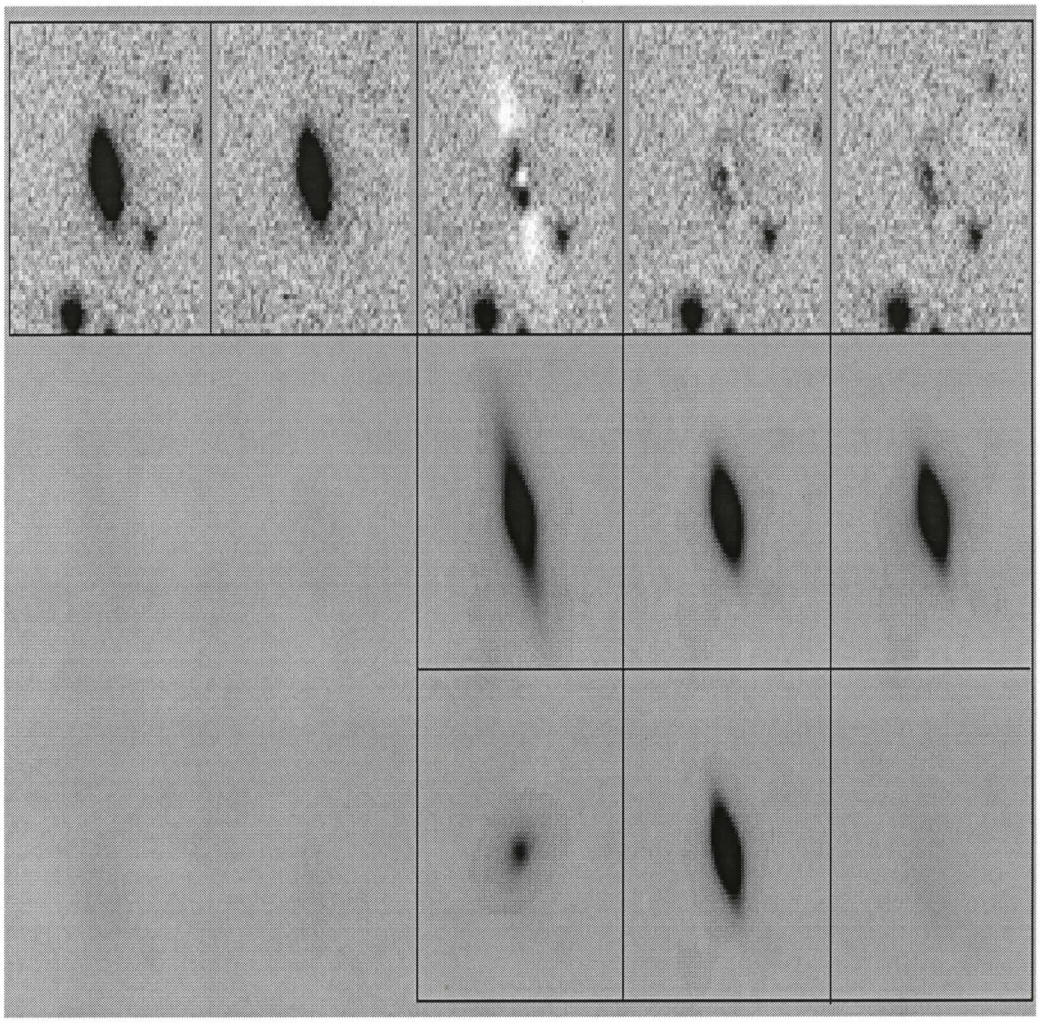

Figure 2.2:

An example of a bulge+disk fit: Top row from left to right: Postage stamp image of galaxy directly from science image, symmetrized image of galaxy with neighbours removed, residual resulting from a bulge model fit to the galaxy, residual from a Disk model fit, residual from a bulge+disk model fit. Second row: bulge model of the galaxy, disk model of the galaxy, bulge+disk model of the galaxy. Bottom row: bulge component of the bulge+disk model, disk component of the bulge+disk model. In this case, as is true for the disks in our sample, the bulge component of the bulge+disk model is a small fraction of the total light for the galaxy. This galaxy has a bulge fraction equal to 9% of the total light.

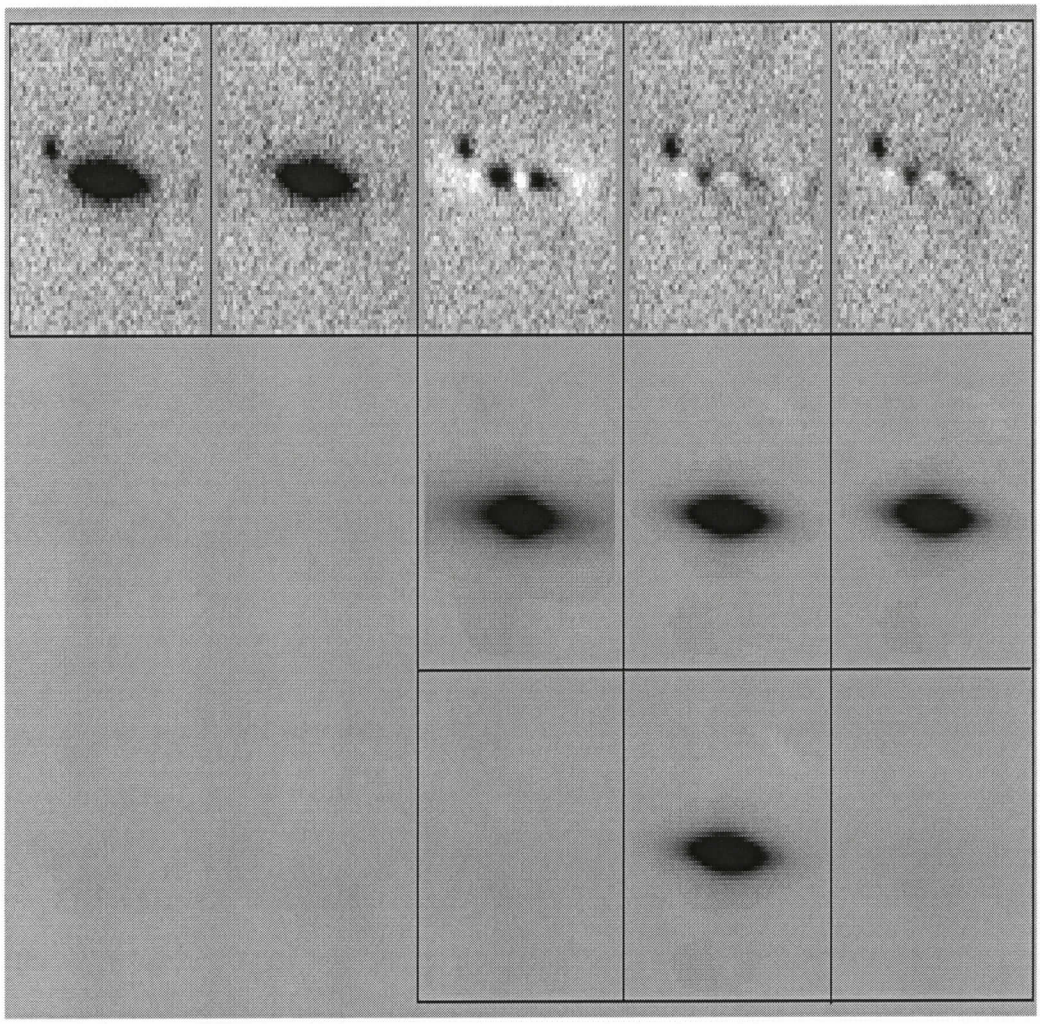

Figure 2.3:

An example of a disk fit: Layout of images is same as Figure 2.2. This galaxy is best fit by a pure disk model. Residual of disk model is the fourth image in the top row and the disk model fit is the second image in the second row. As this image illustrates, the bulge+disk model is reduced to a pure disk model ie. the bulge component is zero. Although in this case the disk model was selected, both models yielded the same parameters for the galaxy, and the χ^2 values between the models differ by less than 1%.

as a function of distance h from the centre:

$$\Sigma(h) = \Sigma_0 exp(-h/h_d) \tag{2.5}$$

where Σ_0 is the central surface brightness of the disk, h_d is the disk scale length where the amount of light in the galaxy drops to $1/e$ of the central value. This is the parameter that will be used in this study as a measure of galaxy size. A composite bulge + disk model is also used where each component is calculated separately and added together. However, these cases are only useful for the purpose of this study when the galaxy is strongly disk dominated.

A small 'postage stamp' image of each galaxy is extracted from the main image for fitting analysis. This allows for faster processing of each galaxy. The routine begins by producing a symmetrized image in order to minimize the effect of asymmetric features or neighbours, as these cannot be modelled. The initial stamp is first rotated by 180^{circ}. This image is then subtracted from the original image and only positive features above 2σ of the noise level are retained in the final frame which is used by the fitting routine (Figures 2.2, 2.3).

The routine typically uses six or seven free parameters for the each of the fits. Typical parameters include centroid, ellipticity, position angle, scale length and bulge fraction. Each component has a different set of parameters that it attempts to fit. As an example, the bulge model will fit the bulge effective radius and the disk model will fit the disk scale length. Each of the above models is convolved with the point-spread function of the image and fit with the parameters relevant to the model in order to minimize the χ^2. Initial values for the centroid and aperture are taken from the SExtractor catalogue. The algorithm begins with an initial value for each parameter it is trying to fit and all parameters are iteratively modified so that the fit proceeds in the direction of lowering the χ^2 of the fit. These initial values can be user defined, but the routine also has its own preset values which are reasonable starting values. The routine repeats this procedure for each of the idealized pure bulge, pure disk and bulge + disk models. It can also generate images of both the

convolved and idealized models based on the fit parameters. These images serve as a useful guide in ensuring that the model with the lowest χ^2 also appears as the best fit (Figure 2.2, Figure 2.3). Although it is not practical for this data set to visually inspect every galaxy as has been done in the past, it is still useful to inspect some subset to ensure that the fitting routine is running properly. A few hundred galaxies were visually inspected in this manner over the course of this study.

2.2.1 Detection Probabilities

The robustness of the fitting software is dependent on the apparent luminosity and size of the measured galaxy. For a given luminosity, a smaller galaxy has a more concentrated light profile whereas a larger one spreads the same amount of light over a greater area. At some level, the light at larger radii will fall below the detection limit. Simulated galaxies are used to find the detection limit and examine the severity of this offset. The simulated galaxies are convolved with a point spread function of one of our science images and added into the science image. The fitting routine is then run on these images, and the measured values are compared to the input values as a function of magnitude. The procedure is performed in an identical manner to that performed in the analysis of the science images.

Detection efficiency of galaxies is examined as a function of size and redshift bin using simulated disk galaxies. The detection efficiency is dependent on two major factors. The galaxy must first be extracted with SExtractor before it can be processed by the fitting routine. The extraction routine will inherently miss galaxies due to crowding or proximity to bright stars. Thus, the detection efficiency will never be 100%. The first value returned is then the probability of SExtractor detecting the galaxy. The surface brightness fitting routine then must return the galaxy correctly as a disk along with the correct size. This value is expressed as the fraction of galaxies that are properly returned. Table 2.2 summarizes the product of these two probabilities. For a given magnitude, detection effiency should decrease

as the size of the galaxy increases. This is because the same amount of light is spread out over a larger area, so the galaxy would eventually become too faint for SExtractor to detect. This effect becomes noticeable at sizes larger than those shown in Table 2.2. Detection efficiency is less than 85% mainly in the smallest size bin. At these sizes, objects could be scattered out of this bin and mistaken for stellar type objects. The detection efficiencies presented in Table 2.2 mainly reflect this scattering effect.

The size range is chosen based on the selection boundaries in luminosity-size space in the highest redshift bin, accounting for the best model of surface brightness evolution. (This will be further described in §2.6 and §3.3). For a given size and redshift bin, the detection efficiency is found by $0.9/p(z, h_d)$ then used as a correction factor for bins that are incomplete. As shown in table 2.2, the correction for incompleteness is generally fairly small. Only the lowest size bin (0.5-1.0) is omitted from further analysis due to incompleteness.

Table 2.2: Detection probability $p(z, h_d)$ for different sizes as a function of redshift

Size (kpc)	$p_{<z>=0.3}$	$p_{<z>=0.5}$	$p_{<z>=0.7}$	$p_{<z>=0.9}$
0.5 - 1.0	0.80	0.7	0.65	0.55
1.0 - 1.5	0.85	0.85	0.8	0.75
1.5 - 2.0	>0.85	0.85	0.85	0.85
2.0 - 2.5	0.85-0.90	0.85-0.90	0.85-0.90	0.85-0.90
2.5 - 3.0	0.85-0.90	0.85-0.90	0.85-0.90	0.85-0.90
3.0 - 3.5	>0.90	>0.90	>0.90	>0.90
3.5 - 4.0	>0.90	>0.90	>0.90	>0.90
4.5 - 5.0	0.91	>0.90	>0.90	>0.90
5.0 - 5.5	0.90	>0.90	>0.90	>0.90

2.3 Disk selection

Disk dominated galaxies are defined as those that are either (1) best fit by a purely disk model or (2) best fit by a bulge plus disk model with a measured bulge to total ratio of less than 0.2. Galaxies that are best fit by a disk model are given a bulge fraction of 0.0. From this sample it is found that most are best fit by a disk model. The 'best fit' is defined as the model which returns the lowest χ^2 value. Visual inspection of a few hundred galaxies revealed that this is a very reliable method. Upon closer examination of our sample, it is found that in some cases the two component model produced a very large value for the scale length of the galaxy, vastly different from that obtained with the corresponding pure disk model. This is due in part to the difficulties involved in separating the two components. This error only occurs for a very small fraction (<1% of the galaxies in the sample of disks). In the case where the bulge+disk model is very strongly disk dominated as in this study, the values should be very close (Figure 2.3). In order to avoid contamination from the few objects that are subject to this error, the following action is taken. When the bulge+disk fit is the selected as the best model for the galaxy, it must also satisfy the constraint that their scale length value is within 25% of the corresponding disk model fit. The 25% value is chosen as it is slightly larger than the errors that are inherent to the fitting routine's measurement of the scale length.

Figure 2.4 shows the luminosity size relationship for different redshift slices. The $1.0 \leq z \leq 1.2$ bin is clearly incomplete. Only the very brightest objects will be detected at this redshift and the choice of filter for disk selection also becomes important. At $z \approx 1$, the 4000 ÅBalmer break is redshifted into redder bandpass. For the sake of completeness the $1.0 \leq z < 1.2$ bin will not be used, and the study will only be conducted to $z = 1$.

Also, the lowest redshift bin appears to exhibit a peculiar distribution with respect to the other redshift bins. The most striking feature here is the presence of

very small high luminosity objects. This will be discussed further in section 2.4.

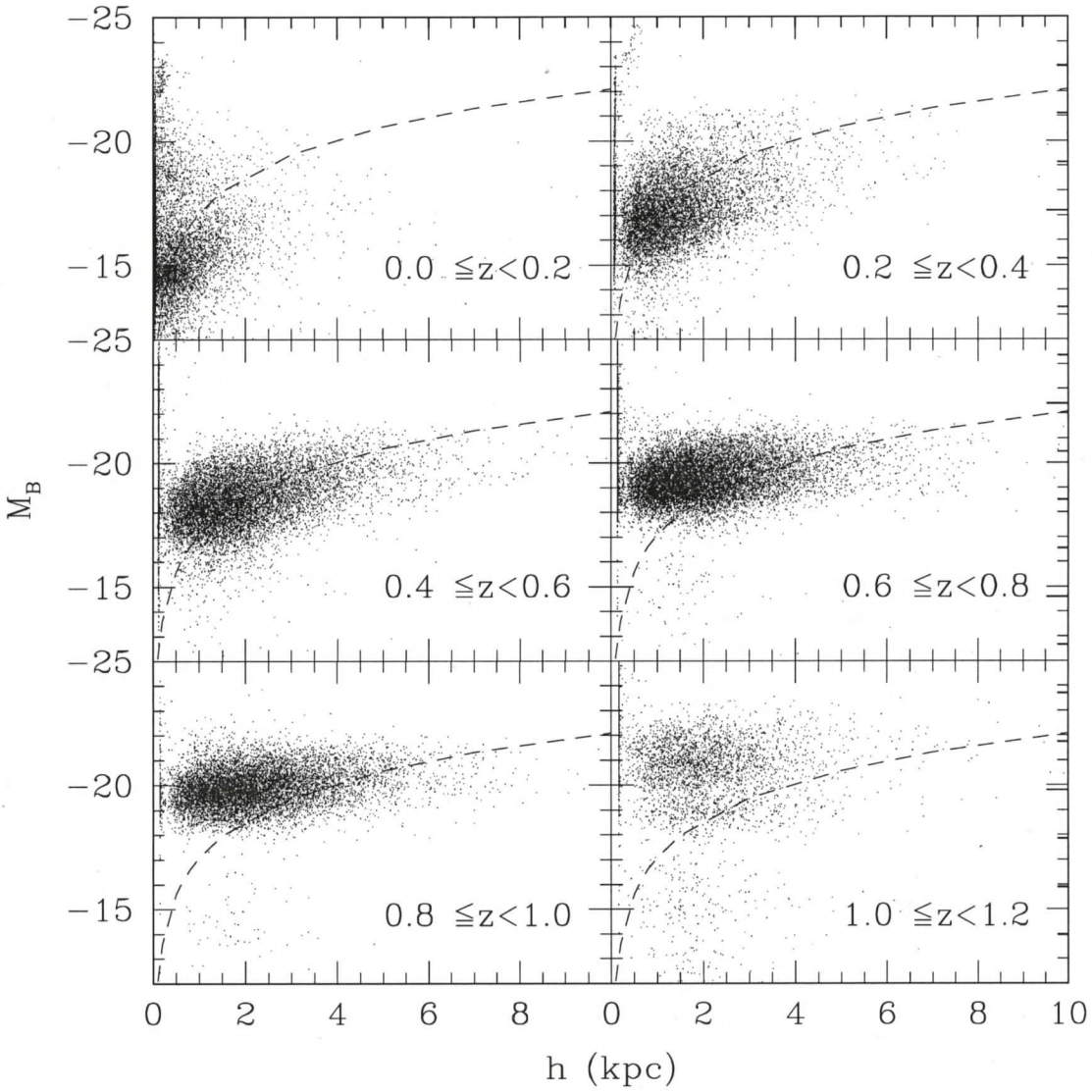

Figure 2.4:

Absolute B band magnitude versus scale length over $0.0 < z < 1.2$: The dashed line shows the Freeman law for local disk galaxies.

2.4 Exploratory Analysis

The Legacy Survey data set poses both a series of blessings and challenges. With the vast number of objects, one should be able to define relationships and trends far better than previous works. However as certain known relationships become clearer with number,unknown ones begin to take shape as well. As Figure 2.4 shows, there is a concentration of small galaxies at high luminosity in the lowest redshift bin that do not appear in other redshift bins. These are clustered around $M_B = -20$. Visual inspection of these objects confirms that they are indeed very small, bright objects and not artifacts. The redshift distribution of Figure 2.6 of objects in this 'clump' show that they are strongly skewed towards lower redshifts in the $z < 0.3$ bin. The spectral energy distributions (SEDs) of these objects show that they have a large drop in U-band flux. There is no such peculiarity in the distribution in the observed space (Figure 2.4). Therefore, it is likely that there has been an error in calculating the redshift. The photometric redshift routine used in this study is constrained to assign values only between 0 and 1.5. Given that the Lyman break lies at $\lambda_0 = 912\mathring{A}$, and the typical redshift for Lyman break galaxies is approximately 3, it is likely that the Lyman break has been redshifted into a longer wavelength bandpass, namely:

$$z = \frac{\lambda - \lambda_0}{\lambda_0}$$
$$\lambda = 3648\mathring{A}$$

which will lie in the Megacam U filter. As the photometric redshift routine tries to match up a template spectra to the galaxy, it will try to match up the Balmer break in the template to the Lyman break in the galaxy SED. Thus, the calculated redshift will be erroneously small. This explains the sudden jump in luminosity in the objects from the main distribution as well as their constraint in redshift space. It is also found that these galaxies are in reasonably good agreement with colour criteria as defined by both LeFévre et al, 2005 and Steidel et al, 2003. All of these

galaxies have $g - r < 1$ and vary in $u - g$ from 1 to about 4. Steidel et al, 2003 classifies Lyman break galaxies (LBGs) as slightly redder than this but also states that there are likely bluer LBGs, but the risk of contamination with stars increases.

Approximately 600 Lyman break galaxies are found to be misidentified as low redshift disks in this study. Another 300 are found to inhabit the same region of luminosity-size space for bulge dominated galaxies.

Steidel et al, 2003 finds that the number density of LBGs is 6052 galaxies/0.9 deg^2, based solely on the photometric criteria of $g-r < 1.2$ and $u-g > g-r+1.5$. Using this criteria, this data set has a similar number density of 6182/0.9 deg^2. In order to avoid contamination from Lyman break galaxies, two actions are taken. The lowest redshift bin $0 \leq z < 0.2$ will not be used in the analysis as the contamination in this bin is most severe. Although this will eliminate most of the LBGs, we do find the presence of LBGs in other redshift bins, using the photometric criteria mentioned above. In each redshift bin beyond $z \geq 0.2$, photometric LBGs make up a small percentage of the bin sample (<8%). In order to minimize the effect of further contamination, the second action taken is to eliminate photometric LBGs from all redshift bins considered in this study. As these objects have improper redshift information, their size and absolute magnitudes are also incorrectly computed. Thus, they appear as very anomalous objects in other redshift bins and are therefore not used.

2.5 The Size Function

The size function (Schade et al, 1995) is used to understand the size evolution of galaxies from $z = 0.2$ to $z = 1.0$. The size function essentially acts as a weighted number density by making use of a galaxy's accessible volume (Section 2.1.4). In a given redshift bin, the $1/V_{max}$ of each galaxy that lies in a given dh_d bin is summed

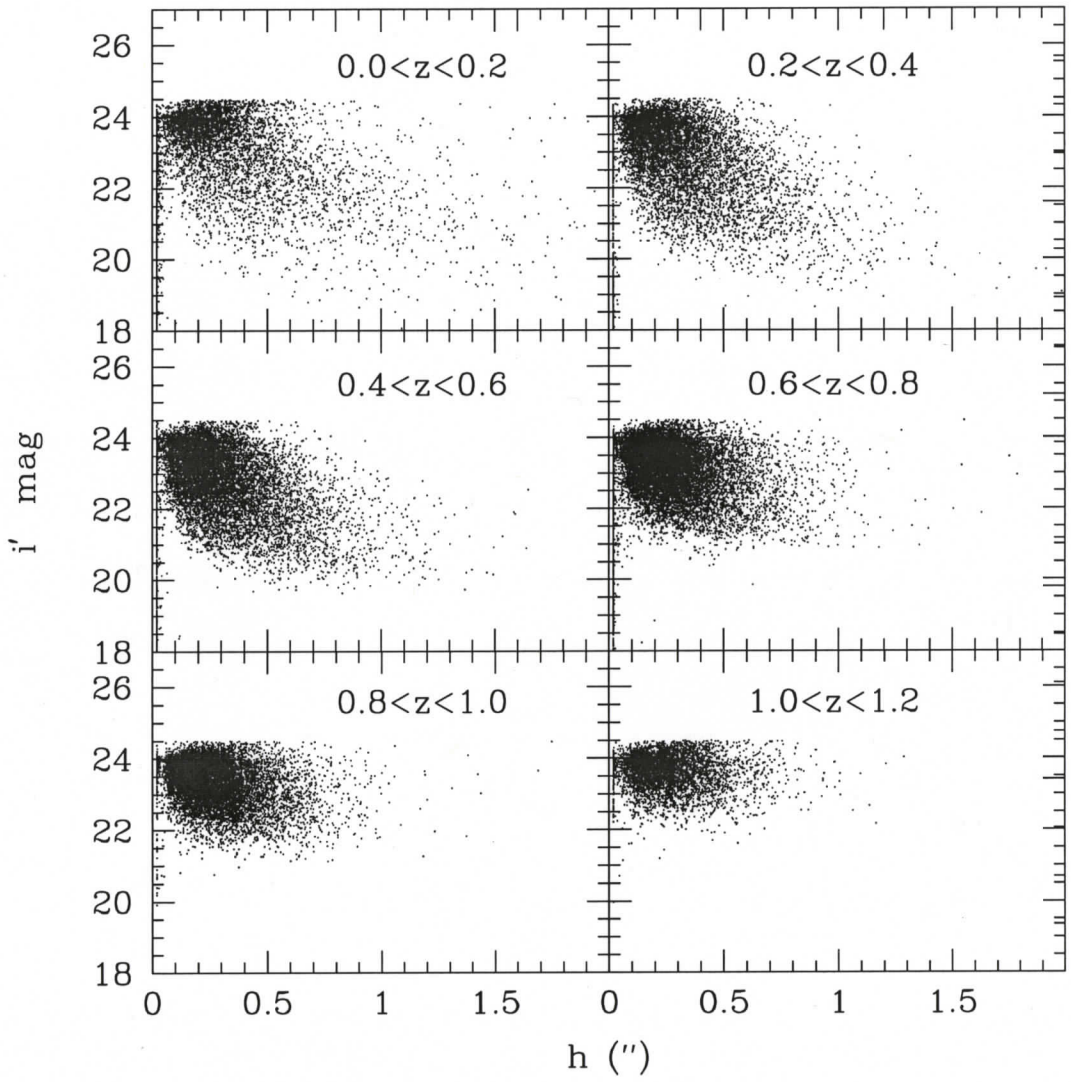

Figure 2.5:

Apparent i' band magnitude vs. apparent size in arcseconds for different redshift slices: Redshift slices do not show a concentration of high luminosity objects. Only galaxies within magnitude limit of survey (i'=24.5) are included.

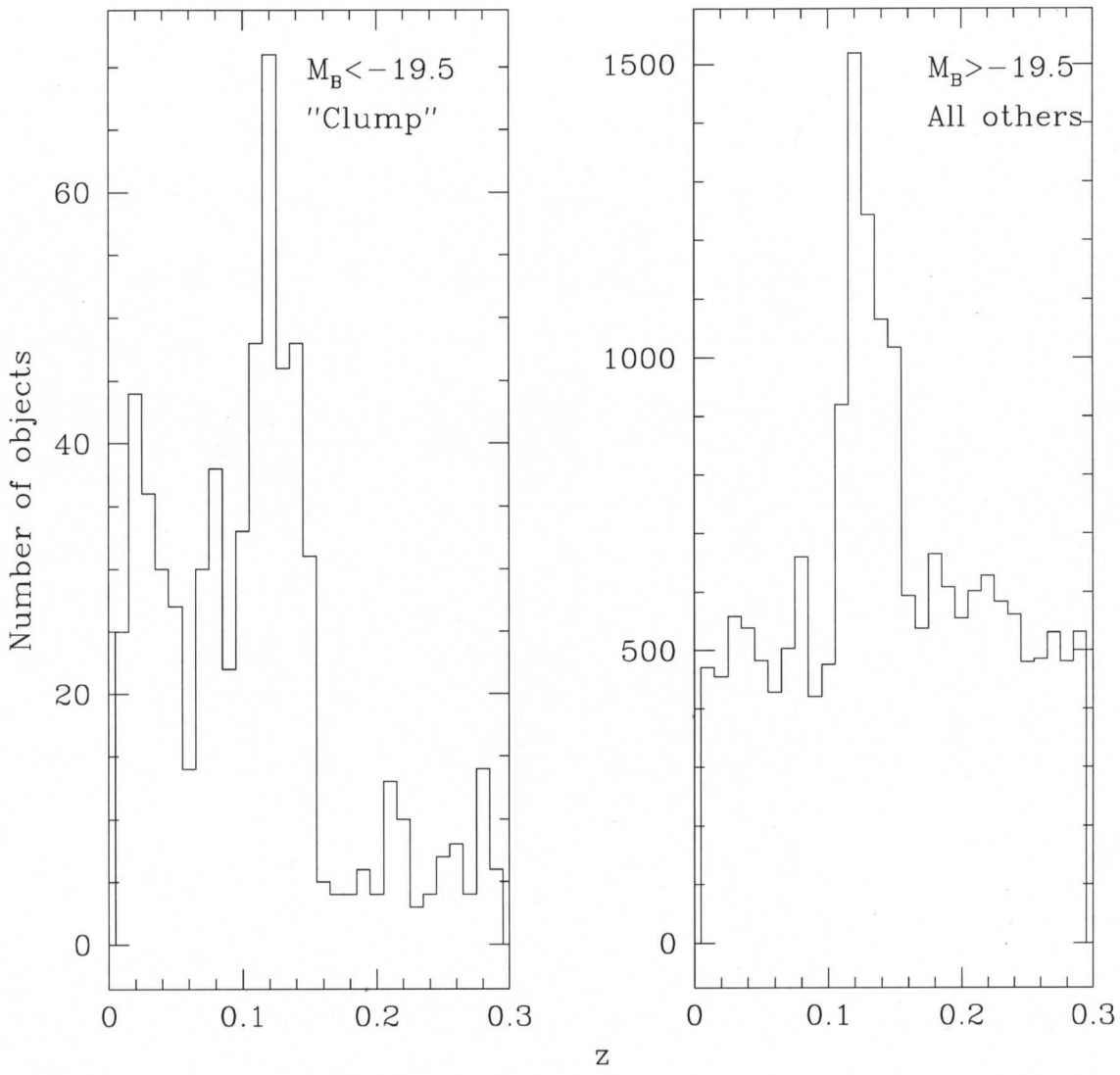

Figure 2.6:

Redshift distribution of Objects in $z < 0.3$: Objects in high luminosity region (M_B >-19.5) are strongly concentrated towards lower redshifts

as follows:

$$\phi(h_d, z)dh_d = \Sigma\frac{1}{V_{max}} \tag{2.6}$$

where h_d is the scale length of the galaxy. The bin widths used in this study are 0.5 kiloparsecs. In this work, intervals of $\Delta z = 0.2$ are used in the computation of the size function. Since the cosmological volume increases with increasing redshift, higher redshift bins contain a larger cosmological volume than lower ones. The $1/V_{max}$ factor acts as a weight to correct for this. A galaxy that is detectable throughout a low redshift bin contributes more to the size function than a galaxy that is detectable throughout a high redshift bin. In the high redshift bin, there are naturally more galaxies due to the increased cosmological volume. Thus there would need to be a corresponding number of galaxies in the highest redshift bin in order to have the same weight as one in the lowest bin in this situation. The size function therefore allows for comparison across all redshift bins despite the increased cosmological volume at higher z.

2.6 Surface Brightness

Another focus of this study is the evolution of surface brightness of disk galaxies. The routine calculates the measured central surface brightness of the disk in magnitudes per square arcsecond. The intrinsic rest-frame B band disk surface brightness of a galaxy is given by:

$$\mu_B = M_B - 2.5log(1 - B/T) + 5logh_d + 38.57 \tag{2.7}$$

where M_B is the absolute B-band magnitude of the galaxy and B/T is the fraction of bulge to total amount of light. Contours of constant surface brightness are straight lines in luminosity-log size space. This will be used to understand the evolution of surface brightness in disks. The approach will be further discussed in section 3.3.

Chapter 3 | *Analysis & Results*

3.1 Quantitative Morphology

Although one would like to believe that nature is orderly and follows predictable patterns, this belief is often met with difficulty. The Hubble classification system (Hubble, 1926) attempts to place galaxies into ordered groups, but there is always undoubtedly a slew of outcasts. Nonetheless, those that can be classified are best done so in a consistent, objective manner. Our academic ancestors tediously pored over photographic plates placing each candidate in its apparent class. It is easy to see that many difficulties would arise with this task as different astronomers would classify galaxies in a slightly different manner (Lahav et al, 1995).

In addition, it is very difficult to pick out certain subtleties about a galaxy's light profile if they are below the threshold of the human eye. Within the last few decades, digital imaging and microprocessors have revolutionized the morphological classification of galaxies by transforming it to a substantially more sophisticated and less subjective process.

Quantitative morphological analysis of galaxies can be done by numerically examining the distribution of galaxy light that is incident upon the CCD detector. From the concentration of light and decomposition of various components, galaxies can be classified based on idealized models.

Despite the elegance of this method, it is misguided to assume that this method is correct in the absolute sense. In order to make a claim about the evolution of a population of galaxies, one must use the same method for the samples being com-

pared. In particular, while studying the evolution of galaxies, it is easy to introduce a bias simply by using different classification or analysis techniques. Thus, any population analyzed using a given technique should only be legitimately compared with another sample using the same technique.

3.2 Measurement biases due to colour

The measurement of the disk galaxy scale length is subject to several possible biases. In this section, some common biases are examined and potential effect on the sample are considered here.

All fitting measurements are performed using only i' band images. This bandpass is selected for several reasons. First, the CFHTLS deep field i' band data has the longest integration time of all the bandpasses used in the survey. Furthermore, the i' band is the least susceptible to dust contamination (Binney & Merrifield, section $\oint$ 4.4.1), as bluer bandpasses are more prone to scattering due to dust. Also, the rest frame i' band measurement is most stable if the galaxy is undergoing star formation in which case the amount of flux through bluer bandpasses will vary more. The use of the i' band filter thus minimizes the potential biases that are far more severe in other bandpasses.

Disk galaxies are also known to exhibit radial colour gradients (de Jong, 1996), which may cause the size measurement to vary as a function of wavelength. These colour gradients are usually due to the concentration of different populations of stars within the galaxy. Older, reddish populations are concentrated in the central bulge, whereas younger, bluer stars inhabit the disk of the galaxy. In a study similar to the one prsesented here, Barden et al, 2005 examined the relative scalelengths of galaxies in various bandpasses with respect to a V band measurement. The motivation was to study the effect of colour gradients. Over the redshift range $0.0 \leq z \leq 1.1$, the correction they applied was $\pm$ 3% based on the study of de

Jong, 1996. Although this value is based on a V-band measurement, this implies that the correction needed from V to I cannot be greater than ± 3%, and the total correction from I to other bandpasses can thus be inferred to be on the order of ± 3%. This is not considered to be a significant effect for the results presented here.

3.3 Selection effects of this sample

When looking at higher and higher redshift objects, only the brightest objects remain detectable and the fainter ones begin to drop out. If not treated properly, this effect can introduce an artifical evolutionary bias into the sample.

In order to evaluate the surface brightness evolution in an unbiased manner across all redshift bins, the size-surface brightness limits of the survey must be established. This is done by constraining the sample to the limits defined in the highest redshift bin. These limits are then applied to all lower z bins as illustrated in Figure 3.1. Galaxies in the highest redshift bin ($0.8 < z < 1.0$) are the most constrained in luminosity-size space with respect to the other redshift bins as only the brightest galaxies remain detectable. Imposing the constraints in luminosity and size as a function of luminosity (surface brightness) present at high redshift on every redshift bin will ensure that the sample used here is free of surface brightness selection biases. This constraint ensures that comparable types of galaxies are used across all redshifts considered. The size function is computed only with the galaxies in this window.

Applying the same 'window' from the highest z bin to all lower bins assumes a no evolution model in the computation of the size function. In order to evaluate the evolution of surface brightness, this window was moved by some magnitude value, and the size function was recomputed. Different values for this offset were tried for each redshift bin, and the size function was recomputed for each different value. As the window was only shifted in magnitude space by some offset, this study only

examines the possibility of pure surface brightness evolution.

3.4 Size function with no evolution

The size function as a function of redshift using equation (2.6) is shown in Figure 3.2. This model assumes no-evolution in surface brightness. The corresponding selection of galaxies for this size function is shown in luminosity-size space in Figure 3.1 as indicated by the no evolution model. Galaxies in this sample are restricted to the luminosity size window in the highest redshift bin. This sample includes approximately 20,000 disk galaxies.

The error bars shown in all the size functions presented in this work are computed using a bootstrap method. The size function is computed 1000 times, each time using a different mock catalog that has been generated from the original sample. The catalog allows for resampling, and the error bars here demonstrate the stability of each value of the size function within the data set. The error bars represent 99% confidence intervals based on the distribution of values produced from repeated calculations of the size function. This is a more time efficient method as it is derived from an existing data set.

From Figure 3.2, it can be seen that all redshift slices display a strikingly similar shape suggesting that the relative distribution of sizes is constant over this redshift range. The size functions of the two highest redshift bins also seem to be in good agreement. However, this size function also demonstrates that the population of disks at $0.8 \leq z < 1.0$ is different from the population at $0.2 \leq z < 0.4$. Several forms of evolution can be considered to explain this effect. It is evident that a simple size evolution model will not suffice. The distribution of sizes in the $0.4 \leq z < 0.6$ is fairly similar to the high z population aside from a slight deficit at small sizes in the $0.4 \leq z < 0.6$ bin. Using a linear shift in size would not reconcile the two distributions. Similarly, it can also be seen that the introduction of size evolution

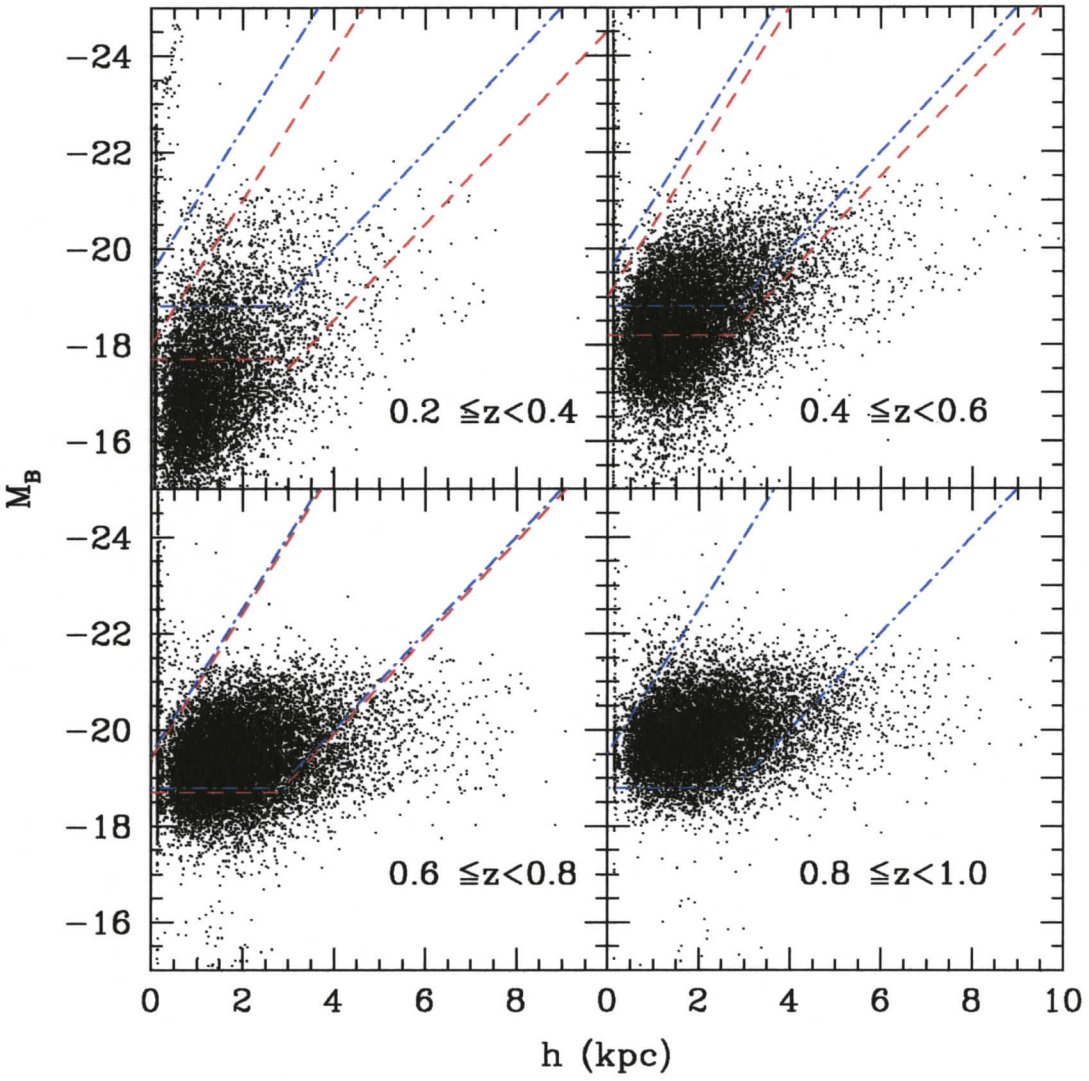

Figure 3.1:

Selected objects in luminosity size space with no evolution and best evolution model: Dot-dashed blue lines indicate the selection window used to compute the size function for the case of no evolution. Dashed red lines in three lowest redshift panels indicate the windows used for the best luminosity evolution model in the computation of the size function. Dot-dashed lines in the highest redshift bin are the same for both no-evolution and best evolution models because size-luminosity constraints from this bin are applied to lower redshift bins.

in the lowest redshift bin would also introduce the same discrepancy at small sizes.

Perhaps the most noticeable effect between the lowest and highest redshift bins is the offset in the size function itself. If, after use of the V_{max} correction, there are simply more galaxies at high redshift then a pure number density evolution model can be considered. However, it can be seen in the two lowest redshift bins that a simple number density shift upward across the entire size distribution would also not adequately describe the evolution present. The number density would need to vary as a function of size. Such models have been proposed (Mao, Mo & White, 1998).

Qualitatively, the pure size or number density evolution models described above do not describe the evolution in the size functions. The next simple model to consider is a pure surface brightness evolution model as described in detail in the following section.

3.5 Size function with surface brightness evolution

The initial size function computed in Figure 3.2 shows the size function under the assumption of no evolution. In this section, an identical analysis is carried out but with various models of surface brightness evolution. The dot-dashed lines in Figure 3.1 demonstrate the selection process of the sample. The luminosity-size space constraints of the highest redshift bin are used to restrict those in other bins and each redshift bin has a different offset in absolute magnitude. In order to assess the surface brightness evolution, a brighter population is selected in each redshift bin, and the size function is recomputed. Various values are tried for each redshift bin and the chi-square value for each evolution model is considered. The size function with the best model for surface brightness evolution is shown in Figure 3.3.

Figure 3.3 clearly shows that the pure surface brightness evolution model is a

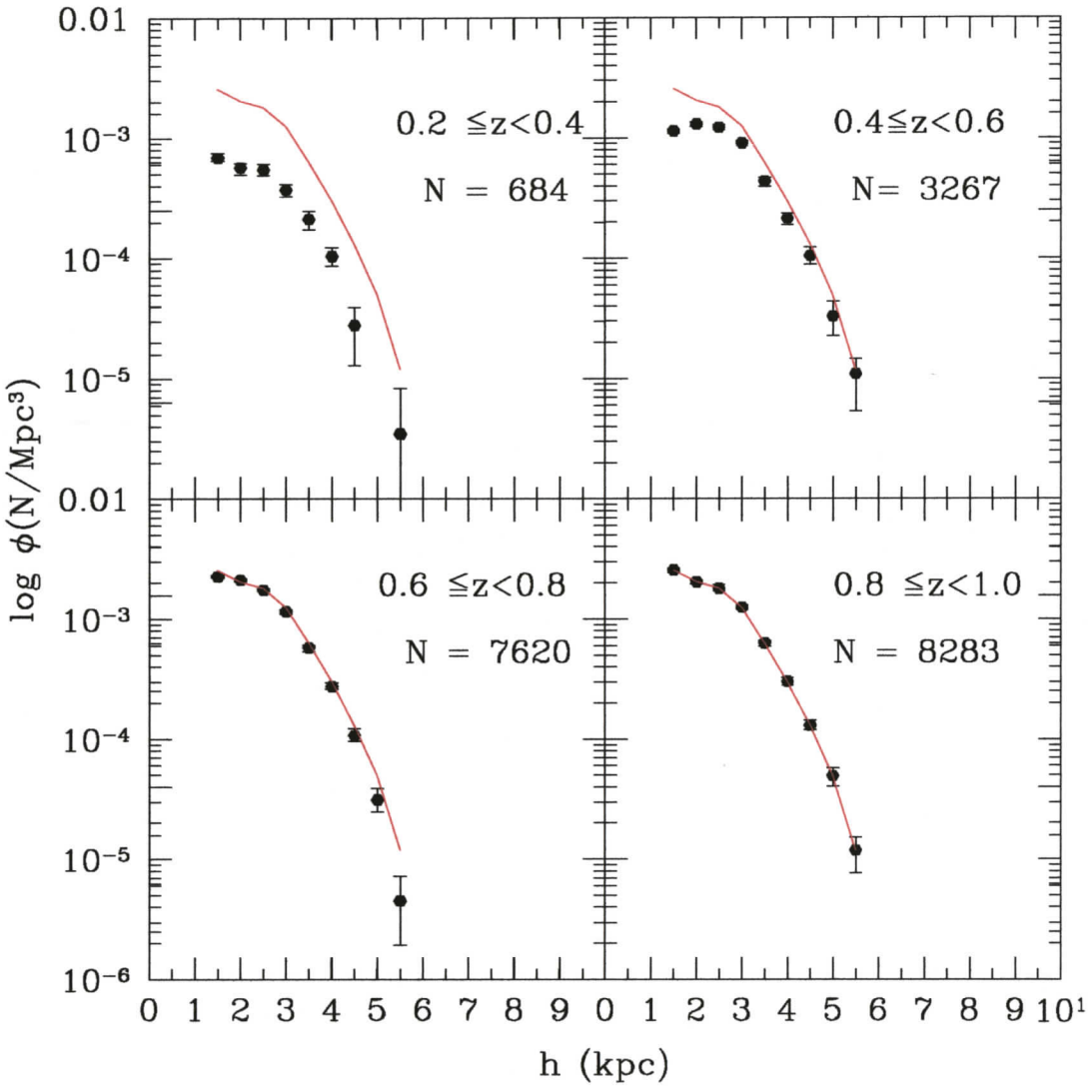

Figure 3.2:

Size function of disk galaxies with no surface brightness evolution: Computed using the galaxies within the blue dashed lines (no evolution model) in Figure 3.1. The red line shows the size function in the $0.8 < z < 1.0$ is reproduced in all other redshift bins.

far better description of the sample than the no evolution model. Each redshift bin is in good agreement in both the size distribution and the number density of the $0.8 < z < 1.0$ population. Although there is some disagreement in the lowest redshift bin, there is only one data point that does not agree with the distribution within the error bars. The simple surface brightness evolution model therefore provides an excellent description of the sample.

In order to quantify the goodness of the surface brightness evolution model, chi-squared is computed as follows:

$$\chi^2 = \Sigma \frac{(y_2 - y_1)^2}{\sigma_2^2 - \sigma_1^2} \tag{3.1}$$

where y_2 is the value of the size function in a given size and redshift bin and y_1 is the value of the size function for the same size bin but a different redshift bin; σ_1 and σ_2 are the errors for the size bin at their respective redshift bins. In addition to the chi-square value, the significance is also computed as outlined in Press et al, 1992. The significance value indicates the probability that the two distributions are drawn from the same parent distribution. A small value of the significance/probability indicates that it is unlikely that the two samples are drawn from the same distribution. In this circumstance, chi-squared is found by comparing each redshift bin to the $0.8 < z < 1.0$ bin.

Table 3.1 illustrates the probabilities for each of the evolved models. The probabilities here indicate the likelihood that the given redshift bin is drawn from the same distribution as the highest redshift bin, $0.8 < z < 1.0$. It is important to note that these distributions assume that there has been no size evolution, thus only testing the likelihood of pure surface brightness evolution over this range.

The hypothesis of no evolution will be taken at a 5% significance level. When the χ^2 probability is greater than 5%, it indicates that this hypothesis cannot clearly be ruled out. For any probability greater than this, the hypothesis that the two populations are drawn from the same distribution is accepted.

From Table 3.1, the best model for surface brightness evolution is found to

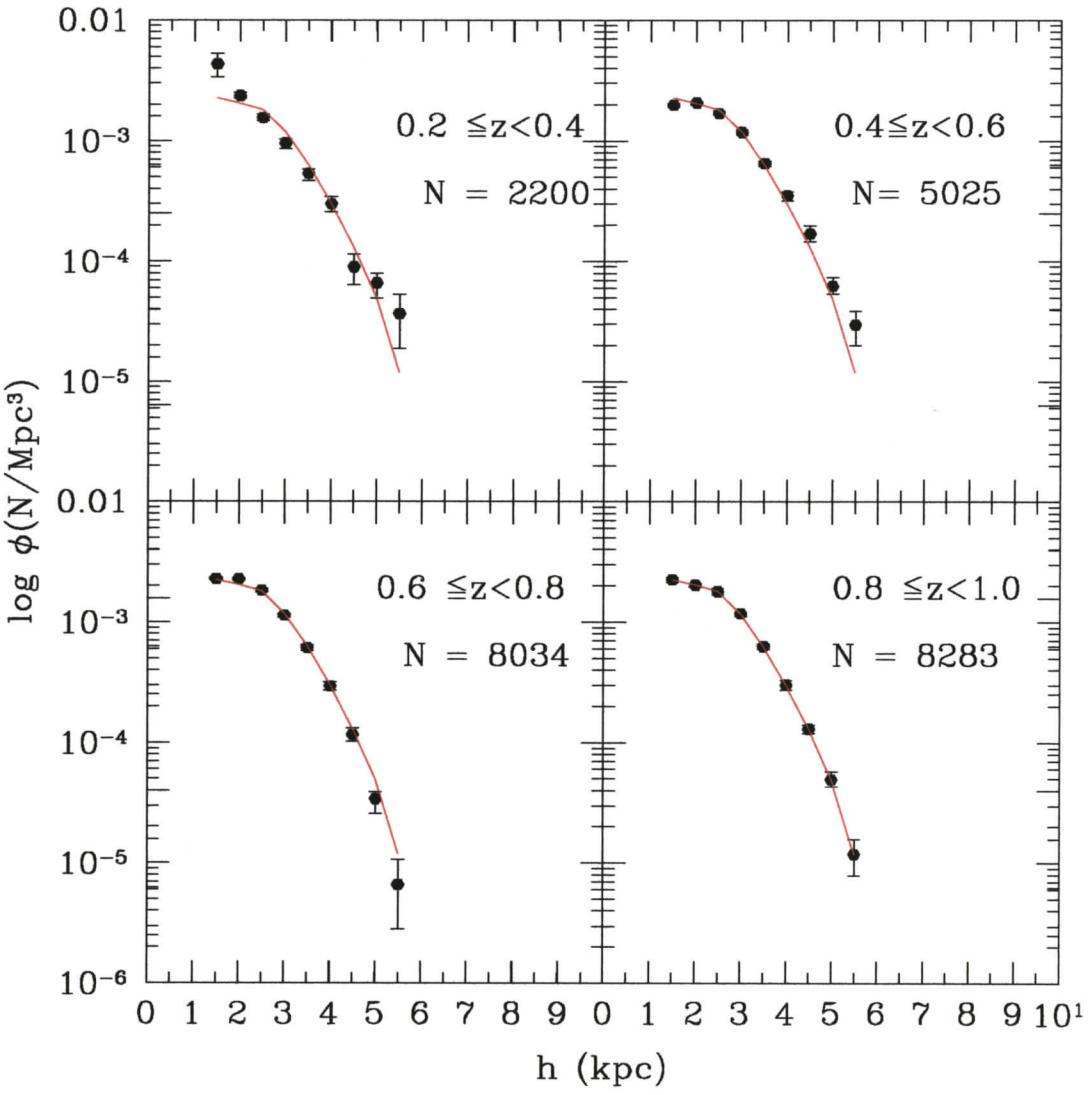

Figure 3.3:

Size function of disk galaxies with 1.5 magnitudes of surface brightness evolution: Computed using galaxies inside red dashed lines in Figure 3.1. These size functions exemplify the best model of surface brightness evolution according to χ^2 probabilities as detailed in Table 3.1. The red line represents the size function at $0.8 < z < 1.0$ and is reproduced in all redshift bins.

be that the population at $< z >= 0.9$ is 1.5 magnitudes brighter than that of $< z >= 0.3$, 0.5 magnitudes brighter than that of $< z >= 0.5$ and 0.1 than that of $< z >= 0.7$. However, at the 5% significance level, several models for each redshift bin can also be accepted. From $< z >= 0.9$ to $< z >= 0.7$ models between 0.0 and 0.3 magnitudes of surface brightness evolution cannot be ruled out. Similarly, for $< z >= 0.9$ to $< z >= 0.5$, models between 0.3 and 0.7 magnitudes are also plausible. From $< z >= 0.9$ to $< z >= 0.3$, 1.2 magnitudes of evolution or greater would be required for the two populations to be drawn from the same distribution. Only the best evolution model is shown in Figure 3.3.

As mentioned in section 3.4, there are several possible physical mechanisms that may explain the evolution seen in figure 3.2. In the above discussion, qualitative arguments show that a pure size or pure number density evolution is not sufficient to reconcile the evolution observed in the size functions. It may be possible that several of these effects are present in varying degrees. This will be discussed further in Chapter 4. Without invoking either of these mixed models this work demonstrates that a simple surface brightness evolution model is sufficient to describe the evolution over this redshift range. This model does not require an evolution in size or number density, and these more complex models are not considered here.

Table 3.1: Probability table for different surface brightness evolution models

z bin –>	$0.2 \leq z < 0.4$		$0.4 \leq z < 0.6$		$0.6 \leq z < 0.8$	
Evolution (mag)	χ^2	Probability	χ^2	Probability	χ^2	Probability
0.0	220.23	9.81E-45	65.210	1.36E-11	4.193	0.7567
0.1	171.20	1.42E-33	31.471	5.08E-08	**2.482**	**0.9281**
0.2	155.57	2.74E-30	21.664	2.90E-03	5.762	0.5649
0.3	123.05	1.77E-23	11.027	0.1375	12.564	0.08341
0.4	126.93	2.75E-24	6.072	0.5314	22.031	0.002515
0.5	79.129	2.07E-14	**3.317**	**0.8542**	31.819	4.38E-05
0.6	64.555	1.88E-11	5.369	0.6150	41.389	6.186E-07
0.7	56.366	7.99E-10	10.974	0.1397	47.321	4.831E-08
0.8	41.549	6.35E-07	18.645	0.00937	61.213	8.638E-11
1.0	25.727	5.65E-04	-	-	-	-
1.2	12.525	0.0845	-	-	-	-
1.3	7.965	0.3357	-	-	-	-
1.4	7.434	0.3852	-	-	-	-
1.5	**5.831**	**0.5588**	-	-	-	-
1.6	6.952	0.4339	-	-	-	-
1.7	7.238	0.4045	-	-	-	-

Chapter 4 | *Discussion*

4.1 Comparison with Previous Observations

With the advent of large, wide-field, ground-based surveys and large space-based projects, the last decade has yielded incredible improvements in the quantity and quality of disk galaxy observations. Clearly, the resulting large samples are the key statistical ingredients needed to understand galaxy evolution. This study presents a sample size that is 1000 times larger than those of ten years ago.

The size function of Figure 3.3 shows that upon assuming 1.5 magnitudes of B-band surface brightness evolution over $0.2 \leq z < 1.0$, no evolution in the size distribution or number density of disk dominated galaxies has occurred over this epoch. Generally, there have been two major conflicting views regarding observations of disks to $z \approx 1$. Although it is mostly agreed upon that there has been minimal size evolution over this period (Ravindranath, 2004, Lilly et al, 1998, Schade et al 1996b, Forbes et al, 1996), the surface brightness evolution has been the topic of much debate. Many works have claimed that there is approximately 1 magnitude of evolution in this time period (Barden et al, 2005, Forbes et al, 1996, Schade et al, 1996b), while others have claimed that there has been little to none (Simard et al, 1999), Ravindranath et al, 2004). Although the sample sizes have been increasing, there is still not a clear value for the amount of surface brightness evolution. Recent observations also come to different conclusions despite this improvement in the observations.

Table 4.1 compares the redshift range and surface brightness evolution found by

various groups over the last decade who have observed populations of disk galaxies.

Table 4.1: Comparison of surface brightness evolution of different works

Group	Number of disks	Redshift Range	μ evolution
Forbes et al, 1996	17	$0.2 \leq z \leq 0.84$	0.6-0.85
Roche et al, 1998	270 [a]	$0.2 \leq z \leq 0.9$	0.94 ± 0.23
Lilly et al, 1998	341	$0.1 \leq z \leq 1$	0.8 ± 0.3
Schade et al, 1996a	110	$0.5 \leq z \leq 1.1$	1.6 ± 0.1
Simard et al, 1999	136	$0 \leq z \leq 1$	minimal
Ravindranath et al, 2004	1508	$0.2 \leq z \leq 1.25$	less than 0.4
Barden et al, 2005	5506	$0 \leq z \leq 1.1$	0.99 ± 0.06 [b]
This Work	20000+	$0.2 \leq z \leq 1.0$	1.5 ± 0.3

[a] to z =3.43
[b] V band

The large spread in surface brightness evolution of different groups in Table 4.1 can be attributed to two main factors. The first is small number statistics. This may affect the results of such studies as Forbes et al, 1996, Schade et al, 1996a where the number of galaxies in each redshift bin is on the order of a handful up to about 20 objects. Clearly, a larger sample is needed to properly evaluate the true average surface brightness at each redshift and subsequently the surface brightness evolution of the disk population. In this respect, the study presented here holds a clear advantage over all previous studies.

The second factor is the bias that arises due to sampling different ranges of surface brightness in different redshift slices. The same faint galaxies in the local universe would not be detected if they were to be placed at high redshift as only the brightest galaxies would remain detectable. One could then make the conclusion that high redshift galaxies are brighter. Without a proper understanding of the selection bias, even a statistically significant sample could classify this effect

as surface brightness evolution. These two effects coupled together could plausibly explain the discrepancy in the values of surface brightness evolution found above. In this study, this bias is approached by limiting the selection of galaxies to that defined in size-luminosity space by the highest redshift bin in the sample. Thus, the surface brightness evolution found in this study is only for galaxies which are detectable throughout the entire redshift range and not subject to the selection bias mentioned above.

Each group's analysis technique must also be taken into careful consideration when comparing the surface brightness evolution values. For example, Ravindranath et al, 2004 use an identical approach to that used here yet they find that there has been no evolution in size or luminosity. If they do not apply any surface brightness restrictions to their sample, they find 0.93 magnitudes of evolution. Ravindranath et al, 2004 present a sizeable sample of approximately 1500 galaxies. However, their lowest redshift bin appears to be subject to small number statistics (although an exact number is not provided, their $0.2 < z < 0.5$ magnitude-size plot is not comparable to that presented here for a similar redshift range) and this leads to a somewhat poorly determined luminosity function for $0.2 < z < 0.5$. Also, their high redshift luminosity function for $1.0 < z < 1.25$ is arguably not very well fit by the non-evolving model as only two of seven data points clearly lie on the model curve within the error bars. However, this is difficult to assess as they do not provide goodness-of-fit parameters. Thus, their claim of no evolution based on their luminosity function requires closer examination.

Barden et al, 2005 carefully examine the selection biases and apply completeness contours to their magnitude-size relation to select unbiased disks. They find that 1 magnitude of luminosity evolution is consistent with their sample to $z = 1.1$, mostly in agreement with what is found in this study. Roche et al, 1998 introduce a combined size-luminosity evolution model which holds out to $z = 4$. Their pure luminosity evolution model predicts a brightening of 0.67 mag to $z = 1$, whereas

their size-luminosity evolution model predicts an evolution of 0.92 magnitudes over the same redshift range. This value is more consistent with their finding of 0.95 magnitudes of surface brightness evolution. Although Barden et al, 2005 and Roche et al, 1998 found similar values for the surface brightness evolution, Barden et al, 2005 did not find it necessary to invoke a size-luminosity evolution model. Barden et al, 2005 does note however that more complex models may also explain the observed evolution, as is noted in this work.

Another potential bias worth mentioning is the possible contamination of other morphological types into each sample. This may cause some discrepancy in the noted surface brightness evolution model. In this study, only strongly disk dominated galaxies are considered. Use of a Sérsic index higher than 1, which may introduce a more prominent bulge component (Ravindranath et al, 2004), or the subjectivity of visual classifications (Roche et al, 1998) may result in a population of disks which are different from those considered here. However, the size-luminosity evolution models of Roche et al, 1998 find similar values for all types of spirals, and the pure luminosity evolution models differ by 0.15 magnitudes between Sab and Sbc galaxies to $z = 1$. Over this redshift range, they note that all morphological types undergo similar luminosity evolution, so this bias is not thought to contribute significantly to the discrepancies in the values noted in table 4.1. Therefore, the analysis technique plays a more significant role.

4.2 Implications regarding evolution of disk galaxies

As a significant fraction of the galaxy population, disk galaxies hold the potential to a better understanding of the mechanisms behind galaxy evolution in general. Under the assumption of 1.5 magnitudes of surface brightness evolution over the redshift range $0.2 \leq z \leq 1.0$, we find that both the size and number density of the

disk population remain essentially constant. This implies that they were already in place before $z = 1$. The fading of the existant stellar population over time through passively evolving stars is thought to account for approximately 1 magnitude of this effect based on model predictions (eg, Bruzual & Charlot, 1993, Trujillo & Aguerri, 2004). However, this work finds a slightly higher value for the evolution. Thus, the remainder can be attributed to stars continuously forming over this epoch. The star formation rate density of the universe is thought to sharply decline at redshifts less than $z = 1.5$ (Madau et al, 1996, Flores et al, 1999, Hammer et al, 1997) thus there is still some amount of star formation present in disks around $z = 1$. With continuous bursts of star formation occurring through this range in redshift, the population would quickly evolve in luminosity. These bursts of star formation quickly fade and evolve passively along with the existant population. This value of evolution is also supported by an analytic model by Naab & Ostriker, 2006. Furthermore, recent smoothed-particle hydrodynamical/N-body simulations of disk galaxies by Brook et al, 2006 predict that the B-band magnitude should change by approximately 1.4 magnitudes over $0 < z < 1$, in accordance with the star formation rates noted above.

The similar size distribution of disks over this redshift follows nicely along with the previous assumption of luminosity evolution. Without any major structural changes, evolution of the disk can only occur with the population of stars already in place. Hierarchical galaxy formation theories predict that disks should be smaller at higher redshift as they are thought to grow larger over time through mergers and gas accretion. The result of an unchanged size distribution is not necessarily in contradiction with this, but implies that one needs to look at higher redshift objects before this trend is more clearly seen. Indeed, high redshift studies have been able to confirm this prediction (Ferguson et al, 2004, Roche et al, 1998), suggesting that most of the size evolution of disks occurs at $z > 1.5$. Furthermore, models also predict that high redshift disks should be denser and possess more concen-

trated surface brightness profiles. In the context of this work, this would suggest an excess of detectable galaxies in the smallest size bins at high z. This effect is not observed. However, this does not mean a catastrophe for ΛCDM hierarchical galaxy formation. Using a magnitude limited survey, Bouwens et al, 2004 found that high redshift ($z \approx 2 - 6$) galaxies tend to be more compact and the incidence of large, low surface brightness galaxies is low.

The above statements are subject to the defintion of a 'disk galaxy'. There is the possibility that some of the larger disks may leave the sample as they merge with other disks possibly forming another galaxy type. In this way, they will be taken out of the sample. However, smaller disks must also be entering the sample in order to preserve the size distribution through cosmological time. Essentially the results of unchanged number density and size distribution are to be understood in the context that there exists similar populations of disks over this redshift range, although they may not necessarily be exactly the same sample under consideration in all redshift slices. In this study, evolution is a statistical change in the distribution of objects rather than the observation of a single galaxy changing in its properties. One must then make the inference that each individual galaxy contributes some amount to this larger statistical change.

Contrary to model predictions of significant evolution occuring over the last 8 billion years, we find that there has been no change in the size distribution or number density over the same time period. This study, when complemented with higher redshift studies, suggests that there is a population of disks to $z = 1$ that were formed at higher redshift.

4.3 Implications for Theoretical Models

This study finds that disk dominated galaxies have not undergone any significant evolution in size since $z = 1$. Across all redshift ranges, the overall size distribution of galaxies at $z = 1$ is found to be similar to the population observed in the present day. These results are inconsistent with model predictions (Mo, Mao & White, 1998, van den Bosch, 1998), as they predict that the disk galaxies must be assembled in recent times (since $z \approx 1$). Their models find that stable disks should only come into existence at $z < 1$. Assuming luminosity evolution, the size function presented here suggests that the distribution of disk sizes remains constant over the same time period and that they were already in place prior to this epoch. However, Mao, Mo & White, 1998 have attempted to reconcile their models with the observations of Schade et al, 1996a and Lilly et al, 1998 which present conclusions similar to this work. They introduce parametrizations where disk scale length evolves as $(1+z)^{-1}$ and where B band luminosity is essentially independent of z. Furthermore, they parametrize the abundance of disks as $(1+z)^3$. They argue that the observations can invoke models other than pure luminosity evolution which are consistent with their parametrizations. Without luminosity evolution, the observations of Schade et al, 1996a could be interpreted as a tenfold increase in the abundance of small disks at high redshift. Using these parametrizations, one arrives at the result that there should be eight times as many small disks at $z = 1$ as the present day. The disks would be about half their current sizes. Although this is not what Schade et al, 1996a concluded, the results could be interpreted as such. In principle this may be worth considering even though it may not necessarily be physically motivated.

The size functions presented in this work also suggest that an increase in number density in smaller disks may explain the evolution over the epoch $0.2 < z < 1.0$. However, this would imply that there has been no luminosity evolution. On the most simplistic level, galaxies must undergo some sort of luminosity evolution as their constituent stellar population ages and thus fades. Fossil studies of local galax-

ies clearly reveal stellar evolution (eg. van den Bergh, 2000). Therefore, it is highly likely that the population has undergone some luminosity evolution as a result of stellar evolution. It is also possible that these effects are both present at varying levels or conspiring to cancel each other in a particular way, but these cases are not considered in this study. In addition to the analytic models presented above, there are a number of N-body models that have attempted to reconcile disk galaxy formation in the context of the ΛCDM paradigm as mentioned in Chapter 1 (Abadi et al, 2003, Steinmetz & Navarro, 1999). The principal problem of these models is the lack of inclusion of realistic feedback processes. Most models do include these processes on some level but the recipes are simplistic and do not seem to be effective enough. This results in early star formation and smaller, more concentrated disks that have a specific angular momentum which is much lower than observed disks of similar rotation speed. Models that incorporate supernovae feedback or suppress cooling to later epochs (Weil, Eke & Efstathiou, 1998, Eke, Efstathiou & Wright, 2000) have been more successful at producing realistic disk galaxies than those mentioned above. As the disk is a fairly fragile object, an early formation would allow it to become more susceptible to disruption in mergers or collisions. Furthermore, these disks are also more prone to significant size evolution after this period as a result of mergers.

Incorporation of models for supernovae feedback and star formation allow the disk galaxy to retain its specific angular momentum during collapse (Thacker & Couchman, 2001, Okamoto et al, 2005 alleviating one of the prinicpal problems of previous models. The effect of feedback is found to regulate the timing of star formation over the history of the galaxy. Rather than a significant period of star formation early in the galaxy's history, the feedback mechanism allow stars to form at lower rates throughout time and also the peak epoch of star formation may be moved to later times, depending on the amount of feedback induced. These models reduce to the case of significant angular momentum transport from baryonic to

dark matter when feedback processes are not included, along with increased star formation rates.

It is clear that current models are lacking vital components. Without an understanding of the balance between feedback processes and star formation, models are unable to produce disks that agree with observations. Numerical modelling of the theoretical picture for hierarchical galaxy formation is subject to a deeper understanding of the physical processes at work as well as an improvement in the resolution. Once these key elements are included, models might then be reasonably compared with observations. In the current state, there is no need to change the hierarchical picture for galaxy formation. Improvements in disk galaxy observations seem to be directing models to a better understanding of the physics rather than a change in the underlying theory.

Chapter 5

Conclusions & Future Work

5.1 Conclusions

In this thesis, data from the Deep component of the Canada-France-Hawaii Telescope Legacy survey was used to trace the size evolution of disk-dominated galaxies out to approximately $z = 1$. A two-dimensional surface brightness fitting routine was used to fit the profiles of the galaxies and determine their morphology. Disk-dominated galaxies were defined as those best fit by a disk model or a two component bulge/disk model with a bulge to disk ratio less than 0.2. Two fields from the survey were used amounting to approximately 2 deg^2. These data allows for remarkable statistical precision over previous works in this field of study. In total, an initial sample of approximately 75,000 disks is compiled using a magnitude limit of i'=24.5. Once the sample is restricted to the region of the luminosity-size space accessible in the highest redshift bin, approximately 20,000 galaxies are left in the sample. The sample is restricted in this manner in order to eliminate possible selection biases due to sampling different surface brightnesses at different redshifts.

The size functions of these disks are consistent with 1.5 $\pm$0.3 magnitudes of B-band luminosity evolution over $0.2 \leq z \leq 1.0$. This simple model does not require an evolution in the size distribution or the number density of disks in these epochs. This result is in agreement with other observational work on disk galaxies, (Trujillo & Aguerri, 2004, Schade et al, 1996a).

The amount of luminosity evolution found in this work is somewhat higher than those of previous works. (Barden et al, 2005, Roche et al, 1998) Taken along with the result of an unchanged size distribution of disks, our result can be interpreted as mostly the passive evolution of the existant stellar population along with some star formation. Observations of high redshift galaxies (Madau et al, 1996, Flores et al, 1999, Hammer et al, 1997) suggest that the star formation rate of the universe peaked around $z = 1.5 - 2$ and is declining in more recent times (Lilly et al, 1996). Thus, the luminosity evolution found in this study can be attributed to both the amount of star formation present in these disks and passively evolving stars.

Although this result is consistent with previous observational studies, it is not in agreement with the models presented in the context of the ΛCDM paradigm, such as those presented by Mo, Mao & White, 1998, van den Bosch, 1998. This study shows that the distribution of galaxy sizes has not changed significantly in the last 8 billion years, suggesting that the population that we observe today was mostly in place by $z = 1$. This result is consistent with the models of Bouwens & Silk, 2002, who suggest a surface brightness evolution of approximately 1.5 magnitudes over the redshift range considered in this study.

Hierarchical galaxy formation predicts that disks should be smaller and more compact than those of today. Given that a population of disks exist in similar number density and size distribution out to $z = 1$, it is likely that the population was in place prior to this. Thus, it is likely that hierarchical mechanisms are more active at higher redshift ($z > 1$) as opposed to the redshift range considered in this study. Complementing this work with observations of higher redshift compact disks (Bouwens et al, 2004, Trujillo et al, 2004) will allow one to make better constraints on the peak epoch of galaxy formation.

5.2 Future Work

The size of the data set presented here allows for the possibility of many exciting studies in the future. Examining the dependence of size and surface brightness evolution on environment would allow one to see if disk galaxies evolve in a different manner when they are isolated, in groups or clusters. Galaxies in highly concentrated regions have a greater probability of interactions or mergers, and this may impact their evolution. Furthermore, existent colour information allows the study of the dependence of the size function with colour and environment. This would allow for a greater understanding of the result obtained here as insight will be gained as to the nature of the stellar populations present at different redshifts. As a simple extension, computing independent size functions for red and blue disks within this sample may reveal whether one group contributes more evolution than the other to the full sample.

Combining this data set with others allows for strong constraints on galaxy evolution. This work demonstrates that disks seem to have been assembled prior to $z = 1$. Examination of disk galaxies at higher redshifts ($z = 2, 3$) would allow one to pinpoint the epoch of peak galaxy evolution. This redshift range can be probed with infrared imaging. A multi-wavelength study of disks would allow for a comprehensive look at the evolution of galaxies over a large range in redshift.

The result of this work demonstrates that the peak epoch of galaxy evolution is still not known and raises further questions about formation times. With better constraints on the epoch of disk formation, observations should be able to piece together a picture of galaxy evolution through cosmological time. Along with better recipes of the physics behind star formation and feedback, theoretical models could help reveal the conditions required to produce galaxies at the correct epoch. Together, these will allow for a deeper understanding of galaxy formation, and their evolution into the captivating structures which stir the curiosity of their observers.

Bibliography

The following abbreviations are used in this bibliography:

MNRAS: Monthly Notices of the Royal Astronomical Society

ApJ: The Astrophysical Journal

ApJ: The Astrophysical Journal Letters

ApJSS: The Astrophysical Journal Supplement Series

AJ: The Astronomical Journal

A&A: Astronomy and Astrophysics

Ap&SS: Astrophysics and Space Science

ARA&A: Annual Reviews of Astronomy and Astrophysics

PASP: Proceedings from the Astronomical Society of the Pacific

Abadi M. G., Navarro J. F., Steinmetz M., & Eke V. R. **2003** ApJ, 591, 499

Barden M., Rix H-W, Somerville R. S., Bell E. F., Huler B., Peng C. Y.; Borch A., Beckwith S. V. W., Caldwell J. A. R., Heymans C., Jahnke K., Jogee S., McIntosh D. H., Meisenheimer K., Sánchez S. F., Wisotzki L. & Wolf C. **2005** ApJ, 635, 959

Bertin E. & Arnouts S **1996** A&AS, 117, 393

Binney J. & Tremaine S. **1987**, *Galactic Dynamics*, Princeton University Press

Binney J. & Merrifield M. **1998**, *Galactic Astronomy*, Princeton University Press

Blumenthal G. R., Faber S. M., Primack J. R. & Rees M. J. **1984**, Nature, 311, 517

Bouwens R. J., Cayòn L. & Silk J. **1997** ApJ, 489, L21

Bouwens R. J., Illingworth G. D., Blakeslee J. P., Broadhurst T. J. & Franx M. **2004**, ApJ, 611, L1

Bouwens R., Silk J. **2002** ApJ, 568, 522

Brinchmann J., & Ellis R. S. **2000** ApJ, 536, 77

Brook C. B., Kawata D., Martel H., Gibson B. K. & Bailin J. **2006**, ApJ, 639, 126

Bruzual A. & Charlot S. **1993** ApJ, 405, 538

Burke B. F. & Graham-Smith F. **1997**, *An Introduction to Radio Astronomy*, Cambridge University Press

Buta R., Mitra S., de Vaucouleurs G., & Corwin H. G. **1994** AJ, 107, 118

Coleman G. D., Wu C. C. & Weedman D. W. **1980** ApJS, 43, 393

de Jong R. S. **1996** A&A, 313, 377

Driver S. P., Fernàndez-Soto A., Couch W. J., Odewahn S. C., Windhorst R. A., Lanzetta K. & Yahil A. **1998** ApJ, 496, L93

Driver S. P., Liske J., Cross N. J. G., De Propris R. & Allen P. D. **2005** MNRAS, 360, 81

Eggen O. J., Lynden-Bell D. & Sandage A. R. **1962** ApJ, 136, 748E

Eke V., Efstathiou G. & Wright L. **2000** MNRAS, 315, L18

Fall M. S., & Efstathiou G. **1980** MNRAS, 193, 189

Ferguson H. C., Dickinson M., Giavalisco M., Kretchmer C., Ravindranath S., Idzi R., Taylor E., Conselice C. J., Fall S. M., Gardner J. P., Livio M., Madau P., Moustakas L. A., Papovich C. M., Somerville R. S., Spinrad H. & Stern D. **2004**, ApJ, L107

Flores H., Hammer F., Thuan T. X., Césarsky C., Desert F. X., Omont A., Lilly S. J., Eales S., Crampton D. & Le Févre O. **1999** ApJ, 517, 148

Forbes D. A., Phillips A. C., Koo D. C. & Illingworth G. D. **1996**, ApJ, 462, 89

Freeman K. **1970** ApJ, 160, 811

Gwyn S. D. J. MSc thesis, University of Victoria, 1995

Hammer F., Flores H., Lilly S. J., Crampton D., Le Févre O., Rola C., Mallen-Orlenas G., Schade D. & Tresse L. **1997**, ApJ, 481

Hammer F., Flores H., Elbaz D., Zheng X. Z., Liang Y. C. & Cesarsky C. **2005** A&A, 430, 115

Heavens A., Painter B., Jiminez R. & Dunlop J. **2004** Nature, 428, 625

Hogg D. W. astro-ph/9905116

Hubble E. P. **1926** ApJ, 640, 321

Kent S. M. **1984**, ApJS, 56, 105

Labbé I., Rudnick G., Franx M., Daddi E. , van Dokkum P. G., Fö rster-Schreiber N. M., Kuijken K., Moorwood A., Rix H., Röttgering H., Trujillo I., van der Wel A., van der Werf P., & van Starkenburg L. **2003** ApJ, 592, L95

Lahav O., Naim A., Buta R. J., Corwin H. G., de Vaucouleurs G., Dressler A., Huchra J. P., van den Bergh S., Raychaudhury S., Sodre L. Jr. & Storrie-Lombardi M. C. **1995** Science, 267, 859

LeFévre O., Paltini S., Arnouts S., Charlot S., Foucaud S., McCracken H. J., Zamorani G., Le Brun V., Maccagni D., Picat J. P., Scaramella R., Scodeggio M., Tresse L., Vettolani G., Zanichelli A, Adami C., Bardelli S., Bolzonella M., Cappi A., Ciliegi P., Contini T., Franzetti P., Gavignaud I., Guzzo L. & Iovino A. **2005** Nature, 437, 519

Lilly S. J., Le Févre O., Hammer F. & Crampton D. **1996**, ApJ, 460, 1

Lilly S. J., Schade D., Ellis R., LeFèvre O., Brinchmann J., Tresse L., Hammer F., Crampton D., Colless M., Glazebrook K., Mallen-Orlenas G., & Broadhurst T. **1998**, ApJ, 500, 75

Lotz J., Madau P., Giavalisco M., Primack J. & Ferguson H.C. **2006**, ApJ, 636, 592

Magnier E. A. & Cuillandre J. C. **2004** PASP, 114, 449

Madau M., Ferguson H. C., Dickinson M. E., Giavalisco M., Steidel C. C. & Fruchter A. **1996**, MNRAS, 283, 1388

Mao S., Mo H. J., & White S. D. M. **1998**, MNRAS, 297, L71

Mo H. J., Mao S., & White S. D. M. **1998**, MNRAS, 295, 319

Naab T. & Ostriker J. P. **2006**, MNRAS, 366, 899

Nüijten M. J. H. M., Simard L., Gwyn S., Röttgering H. J. A. **2005** ApJ, 626L, 77N

Okamoto T., Eke V. R., Frenk C. S. & Jenkins A. **2005** MNRAS, 363, 1299

Peng C. Y.; Ho L. C. Impey C. D. Rix H.-W. **2002**, AJ, 124, 266

Poggianti B. M. & Barbaro G. **1997** A&A, 325, 1025

Press W. H., Teuloksky S. A., Vetterling W. T. Flannery B. P. *Numerical Recipes in Fortran 77: The Art of Scientific Computing, 2nd Edition* **1992**, Cambridge University Press, Cambridge

Press W. H. & Schechter P. **1974** ApJ, 187, 425

Ravindranath S., Ferguson H. C., Conselice C., Giavalisco M., Dickinson M., Chatzichristou E., de Mello D., Fall S. M., Gardner J. P., Grogin N. A., Hornschemier A., Jogee S., Koekemoer A., Kretchmer C., Livio M., Mobasher B. & Somerville R. **2004** ApJ, 604, L9

Robertson B., Cox T. J., Hernquist L., Franx M., Hopkins P. F., Martini P. & Springel V. **2006**, 641, 21

Roche N., Ratnatunga K., Griffiths R. E., Im M. & Neuschaefer L. **1996** MNRAS, 282, 1247

Roche N., Ratnatunga K., Griffiths R. E., Im M. & Naim A. **1998** MNRAS, 293, 157

Schade D., Barrientos L. F. & López-Cruz O. **1997** ApJ, 477, L17

Schade D., Carlberg R. G., Yee H. K. C., López-Cruz O & Ellingson E. **1996** ApJ, 103, L103

Schade D., Lilly S. J., Le Fevre O., Hammer F. & Crampton D. **1996** ApJ, 464, 79

Schade D., Lilly S. J., LeFèvre O.,Hammer F. & Crampton D. **1995**, ApJ, 451, 1

Schaeffer R. & Silk J. **1988** ApJ, 332, 1

Schmidt M. **1968** ApJ, 151, 393

Shen S., Mo H. J., White S. D. M., Blanton M. R., Kauffman G., Voges W., Brinkmann J. & Csabai I. **2003** MNRAS, 343, 978

Silk J. & Bouwens R. 'Galaxy Formation' *Encyclopedia of Astronomy & Astrophysics*, Institute of Physics Publishing, Bristol & Philadelphia, 2006

Searle L. & Zinn R.**1978** ApJ, 225, 334

Simien F. & de Vaucouleurs G. **1986** ApJ, 302, 564

Simard L., Willmer C. N. A., Vogt N. P., Sarajedini V. L., Phillips A. C., Weiner B. J., Koo D. C., Im M., Illingworth G. D. & Faber S. M. **2002**, ApJS, 142, 1

Simard L., Koo D. C., Faber S., Sarajedini V. L., Vogt N. P., Phillips A. C., Gebhardt K., Illingworth G. D., & Wu K. L. **1999**, ApJ, 519, 563

Springel V. & Hernquist L. **2005**, ApJ, 622, 9

Steidel C. C., Adelberger K. L., Shapley A., Pettini M., Dickinson M. & Giavalisco M. **2003** ApJ, 592, 728

Stetson P. B. **1987** PASP, 99, 191

Sommer-Larsen J., Götz M. & Portinari L. **2003** ApJ, 596, 47

Sommer-Larsen J. & Dolgov A. **2001** ApJ, 551, 608

Steinmetz M., & Navarro J. F. **1999** ApJ, 513, 560

Steinmetz M., & Navarro J. F. **2002** New Astronomy, 7, 155

Thacker R. J. & Couchman H. M. P. **2001** ApJ, 555, L17

Tóth G. & Ostriker J. P. **1992** ApJ, 389, 5

Trujillo I., Aguerri J. A. L., Cepa J. & Gutiérrez C. M. **2001**, MNRAS 328, 977

Trujillo I. & Aguerri J. A. L. **2004** MNRAS, 355, 82

Trujillo I., Rudnick G., Rix H.-W., Labbé I., Franx M., Daddi E., van Dokkum P. G., Förster Schreiber N. M., Kuijken K., Moorwood A., Röttgering H., van de Wel A., van der Werf P. & van Starkenburg L. **2004**, 604, 521

van den Bergh S. *The Galaxies of the Local Group*, Cambridge University Press **2000**, Cambridge

van den Bosch F. C. **1998** ApJ, 507, 601

Vogt N. P., Forbes D. A., Phillips A. C., Gronwall C., Faber S. M., Illingworth G. D. & Koo D. C. **1996** ApJ, 479, L121

Weil M. L., Eke V. R. & Efstathiou G. **1998** MNRAS, 300, 773

White S. D. M. & Rees M. J. **1978** MNRAS, 183, 341